On the theory of dislocation and generalized disclination fields and its application to straight and stepped symmetrical tilt boundaries

Claude Fressengeas, Xiaoyu Sun

On the theory of dislocation and generalized disclination fields and its application to straight and stepped symmetrical tilt boundaries

[1]Claude Fressengeas, [2]Xiaoyu Sun
[1]Laboratoire d'Etude des Microstructures et de Mécanique des Matériaux, LEM3, Université de Lorraine/CNRS/Arts et Métiers ParisTech
7 rue Félix Savart, 57070 Metz, France
[2]PengCheng Laboratory, 2 Xingke 1^{st} Street, Nanshan, Shenzhen 518055, China

July 18, 2020

Abstract

The theory of dislocation and generalized dislocation fields is developed within a second-order mechanical framework where the description of the internal state of the body and the balance equations involve the stress and hyper-stress tensors, work-conjugates to the strain and second-order distortion tensors. Consistently, the free energy density depends on the elastic strain and second-order distortion tensors. To obtain a continuous setting, the theory uses the duality between the discontinuity of the elastic displacement vector and distortion tensor fields and the incompatibility of the smooth second-order elastic distortion field. The conservation of these discontinuities across arbitrary patches provides transport relationships for the motion of dislocations and generalized disclinations serving as a kinematic basis for the description of plasticity and phase transformation. Closure of the theory derives from constitutive relationships for the mobility of dislocations and generalized disclinations compatible with the thermodynamic requirement of positive dissipation. In contrast with dislocations, the driving forces for generalized disclinations involve the hyper-stress tensor, not the stress tensor. The resulting theory is able to address boundary value problems for the elasto-plasticity of solids coupled with phase transformation along arbitrary loading paths. We provide examples showing generalized disclination distributions in plane state situations such as straight symmetrical tilt boundaries and symmetrical tilt boundaries involving steps and ledges.

1 Introduction

Engineering situations where the elastic displacement field presents discontinuities across bounded surfaces are commonplace in deforming solids. They include grain boundaries and triple lines, inclusions in a matrix of dissimilar material, shear bands, incoherent interfaces, twinning and phase transformation interfaces (interphases), etc. Crystal defect models such as dislocations and disclinations were simultaneously defined by Volterra [1907] early in the last century to account for bounded displacement discontinuities in solids. In the sole presence of a dislocation, the elastic displacement vector field encounters a constant discontinuity across some surface S bounded by the dislocation line. A translation takes place across S, while continuity of the elastic strain and rotation is maintained. The discontinuity of the elastic displacement induces an incompatibility of the elastic strain tensor, reflected in a non-vanishing tensor field of crystal defect densities $\boldsymbol{\alpha}$ referred to as Nye's tensor of dislocation densities in the elastic theory of continuously distributed dislocations (ECDD) [Nye, 1953; Kondo, 1953; Bilby et al., 1955; Kröner, 1981]. In ECDD, the elastic curvature tensor is defined as the gradient of the elastic rotation vector, and it is therefore compatible. Nevertheless, it contributes to the incompatibility reflected in Nye's tensor $\boldsymbol{\alpha}$. When the elastic rotation vector/tensor fields additionally present a constant discontinuity across S, the elastic curvature tensor field also turns out to be incompatible, and the discontinuity of the displacement field has rigid-body character [Weingarten, 1901; Volterra, 1907]. Such a situation is typically met in polycrystals, across grain and subgrain boundaries. The incompatibility of curvature is reflected in the disclination density tensor field $\boldsymbol{\theta}$ [deWit, 1970], which complements the dislocation density tensor $\boldsymbol{\alpha}$ in the description of lattice incompatibility. The $(\boldsymbol{\alpha}, \boldsymbol{\theta})$ defect densities and displacement fields are then described by the elastic field theory of dislocations and disclinations of deWit [1970], which reduces to ECDD when $\boldsymbol{\theta} = 0$.

Beyond Volterra's construct and in addition to discontinuities of the elastic displacement and rotation tensor (the skew-symmetric part of the elastic distortion tensor), the elastic strain tensor, *i.e.* the symmetric part of the elastic distortion tensor, may also encounter discontinuities across bounded surfaces in the body. Then, the discontinuity of the elastic displacement field is not that of a rigid body as in Weingarten's theorem, but of a deforming body. As shown in [Acharya and Fressengeas, 2012], the discontinuity of the (first-order) elastic distortion translates into the incompatibility of the second-order elastic distortion (*i.e.* the second gradient of the elastic displacement in compatible elasticity), and into the existence of a non-vanishing third-order tensor field of crystal defect densities $\boldsymbol{\pi}$, referred to in this paper as the generalized disclination ("g-disclination") density tensor field. This tensor degenerates into the standard disclination density tensor $\boldsymbol{\theta}$ when the elastic strain tensor retains continuity. It vanishes when the discontinuity of the elastic displacement is a mere translation.

In this paper, we present a linearized theory of the anelastic dynamic behavior of incompatible media containing dislocations and g-disclinations subjected to arbitrary loading paths. To describe the internal mechanical state of the body, the theory involves the stress and second-order stress ("double-stress" or "hyper-stress") tensors as work-conjugates to the strain and second-order distortion tensors. Similar theories were presented in [Acharya and Fressengeas, 2012, 2015], but the choice was made therein to use the couple-stress theory of Mindlin and Tiersten [1962] for this description, leading to some restrictions in the applied loading. In this presentation, the mechanical equilibrium equations involve both the symmetric and skew-symmetric parts of both the stress and hyper-stress tensors, in a setting proposed by Mindlin and Eshel [1968]. The free energy density is assumed to be a second degree polynomial of the elastic strain and second-order distortion (*i.e.* strain-gradient and curvature) tensor fields. Thus, the elastic constitutive laws are linear, but non-local in the presence of generalized disclinations. As is customary in the thermodynamics of continuous media [Coleman and Gurtin, 1967], the elastic constitutive laws will be identified by demanding vanishing dissipation in all reversible processes, and the mobility laws restricted by further requiring that defects mobility warrant non-negative dissipation. As limiting cases, the theory should contain the earlier mechanical field theory of dislocations [Acharya, 2001] when the elastic second-order distortion is compatible, and the theory of dislocations/disclinations [Fressengeas et al., 2011] when only the symmetric part of the latter (*i.e.* the strain-gradient) is compatible. In the absence of both dislocations and disclinations, it should also reduce to the gradient theory of compatible elasticity of Mindlin and Eshel [1968].

This paper is primarily concerned with continuous modeling at nanoscale of crystal defects and crystal defect ensembles, particularly grain and phase boundaries. Models involving statiscally stored dislocations are unfit for such small-scale analyses, although the microstructure and dynamics of these crystal defect ensembles have far-reaching effects on the macroscopic properties of polycrystalline materials. Earlier continuum mechanics models have dealt with coherent or incoherent grain boundaries, using interfacial elements with phenomenological prescriptions deriving from atomistic or dislocation dynamics calculations [Warner et al., 2006; Zbib et al., 2011], or surface-dislocation distributions, see *e.g.* [Berbenni et al., 2013; Vattré, 2017a,b]. However, in contrast with the present approach, these authors did not use continuous dislocation and g-disclination fields in this description, nor did they account for the elastic/plastic distortion incompatibility taking place at grain boundaries. Consequently, while these models can reproduce some of the features of grain boundaries, they cannot account for their core structure and core mechanisms such as the absorption/emission of dislocations. By using the theory of dislocation fields [Acharya, 2001], the incompatibility of the (first-order) elastic/plastic distortion was accounted for at mesoscale along grain boundaries in Fressengeas [2019]; Fressengeas and Upadhyay [2020], implying Burgers vector conservation and tangential continuity of the elastic/plastic distortion across static boundaries or boundaries propagating normally

to themselves. The presence over a finite-width layer across the boundary of continuous dislocation distributions allowed for the description of boundary curvature [Fressengeas, 2019] and of slip transfer [Fressengeas and Upadhyay, 2020], but second-order distortion incompatibility is needed for the description of core properties at nanoscale. Continuous core description of symmetrical tilt grain boundaries were given in [Taupin et al., 2013; Fressengeas et al., 2014; Cordier et al., 2014] using the elasto-plastic theory of dislocation and disclination fields [Fressengeas et al., 2011, 2012] and in [Cleja-Tigoiu et al., 2019]. In these papers, grain boundaries were seen as periodic arrays of disclination dipoles distributed over a thin layer, for example a few Å thick in Cu [Taupin et al., 2013; Fressengeas et al., 2014]. A continuous distribution of the elastic energy arising from the associated incompatible strains and curvatures was obtained in this area. Accounting for rotational incompatibility allowed for a stable defect core structure, and dislocation-grain boundary interactions could therefore be described [Taupin et al., 2017]. Further, plasticity mechanisms such as grain boundary migration were explained in terms of coupled transport of dislocation and disclination densities. However, incoherent interfaces and phase boundaries, or grain boundaries with steps or ledges, were beyond the scope of these investigations, because they involve discontinuities of the elastic/plastic strain across the boundary. The present dislocation and generalized disclination theory is used in the following to extend this approach to non-planar interfaces showing steps and ledges, thus opening the way to dealing with curved interfaces and dilation-retraction mechanisms at interfaces. Symmetrical tilt boundaries are chosen for simplicity. The paper then proceeds in three steps. Firstly, we detail a plane restriction of the theory sufficient for symmetrical interfaces. We show the role of generalized disclinations in this context, and illustrate the differences between the "couple-stress" Mindlin-Tiersten and "hyper-stress" Mindlin-Eshel treatments. Secondly, we discuss the shear strain discontinuities revealed by Couillard et al. [2013] in straight symmetrical tilt boundaries. These features cannot easily be accounted for in dislocation/standard disclination theories, and they are interpreted here in terms of generalized disclination dipoles. Finally, the elastic structure of steps and ledges is detailed in terms of elastic stretch and rotation discontinuities, and described using the associated generalized disclination dipoles. In addition to providing a realistic description of the structure of tilt boundaries and showing the contributions of generalized disclinations to the latter, specific objectives of this presentation include evidencing the benefits offered by a continuous rendition of lattice incompatibility below inter-atomic spacing and by accounting for the non-locality of the elastic response in the core region of the boundaries through second-order distortions.

The paper is organized as follows. Notations are settled in Section 2. Incompatibility in the theories of dislocations and g-disclinations is reviewed in Section 3. In Section 4, transport properties are presented. Section 5 deals with second-order equilibrium equations and boundary conditions. The elastic constitutive relations appropriate for second-order incompatible media are detailed in Section 6, where thermodynamic

guidance following from dissipation arguments is also used to derive driving forces and admissible mobility laws for dislocation and g-disclination motion. Section 7 provides algorithms for the solution of boundary value problems in the elasto-static and anelastic dynamic configurations. In Section 8, a plane dislocation/g-disclination model adequate for the description of symmetrical tilt boundaries is presented, and the relevance in this description of both the Mindlin-Eshel mechanical framework and the g-disclination concept is shown from examples of planar and non-planar symmetrical tilt boundaries. A summary and concluding remarks follow.

2 Notations

A bold symbol denotes a tensor, as in: $\mathbf{A}$. When there may be ambiguity, an arrow is superposed to represent a vector: $\vec{\mathbf{V}}$. All tensor subscripts refer to the basis $(\mathbf{e}_i, i = 1, 2, 3)$ of a rectangular Cartesian coordinate system. Vertical arrays of one, two or three dots represent contraction of the respective number of "adjacent" subscripts on two immediately neighboring tensors, in standard fashion. For example, the tensor $\mathbf{A}.\mathbf{B}$ with components $A_{ik}B_{kj}$ results from the dot product of tensors $\mathbf{A}$ and $\mathbf{B}$, and $\mathbf{A} : \mathbf{B} = A_{ij}B_{ij}$ represents their inner product. The inner product of two third order tensors is denoted $\mathbf{A}\vdots\mathbf{B} = A_{ijk}B_{ijk}$. The cross product of a second or third-order tensor $\mathbf{A}$ and a vector $\mathbf{V}$, the **div** and **curl** operations for second and third-order tensors are defined row by row, in analogy with the vectorial case. For example:

$$
\begin{aligned}
(\mathbf{A} \times \mathbf{V})_{ik\,or\,ijk} &= e_{klm}A_{il\,or\,ijl}V_m && (1)\\
(\mathbf{div}\,\mathbf{A})_{i\,or\,ij} &= A_{ik,k\,or\,ijk,k} && (2)\\
(\mathbf{curl}\,\mathbf{A})_{ik\,or\,ijk} &= e_{klm}A_{im,l\,or\,ijm,l}. && (3)
\end{aligned}
$$

where e_{jkl} is a component of the third-order alternating Levi-Civita tensor $\mathbf{X}$. The comma preceding a subscript indicates a spatial derivative with respect to the corresponding coordinate. The curl tensor may also be seen as the inner product of the gradient tensor with the alternator $\mathbf{X}$, with changed sign:

$$\mathbf{curl}\,\mathbf{A} = -\mathbf{grad}\,\mathbf{A} : \mathbf{X}. \tag{4}$$

A vector $\vec{\mathbf{A}}$ is associated with tensor $\mathbf{A}$ by using the inner product of $\mathbf{A}$ with tensor $\mathbf{X}$:

$$
\begin{aligned}
(\vec{\mathbf{A}})_k &= -\frac{1}{2}(\mathbf{X} : \mathbf{A})_k = -\frac{1}{2}e_{kij}A_{ij} && (5)\\
(\mathbf{A})_{ij} &= -(\mathbf{X}.\vec{\mathbf{A}})_{ij} = -e_{ijk}(\vec{\mathbf{A}})_k. && (6)
\end{aligned}
$$

Similarly, alternating the third order tensor $\mathbf{B}$ by $\mathbf{X}$ produces the second order tensor $\mathbf{A}$ as in:

$$(\mathbf{A})_{ij} = -\frac{1}{2}(\mathbf{X} : \mathbf{B})_{ij} = -\frac{1}{2}e_{ikl}B_{klj}, \tag{7}$$

and conversely, alternating back the second order tensor $\mathbf{A}$ yields tensor $\mathbf{B}$:

$$(\mathbf{B})_{ijk} = -(\mathbf{X}.\mathbf{A})_{ijk} = -e_{ijl}A_{lk}, \tag{8}$$

The symmetric and skew-symmetric parts of tensor $\mathbf{A}$ are denoted $\mathbf{A}^{sym}$ and $\mathbf{A}^{skew}$ respectively. The deviatoric and hydrostatic parts are respectively $\mathbf{A}^{dev}$ and $\mathbf{A}^{hyd}$. In the present paper, symmetry and skew-symmetry of third order tensors relate to the first two subscript positions. For example: $A^{sym}_{ijk} = A^{sym}_{jik}$. A superposed dot represents a material time derivative.

3 Compatibility vs. incompatibility in the theory of crystal defects

3.1 Review of compatibility theory

In a simply-connected body D undergoing a continuous elasto-plastic deformation process, the displacement vector field $\mathbf{u}$ and the rotation vector field

$$\vec{\boldsymbol{\omega}} = \frac{1}{2}\,\mathbf{curl}\,\mathbf{u} \tag{9}$$

deriving from this displacement are single-valued at any point and possibly defined between the atoms, below inter-atomic distances. Therefore, the conventional compatibility conditions on distortion, rotation, strain and curvature should be satisfied. If $\mathbf{I}$ denotes the identity tensor, $\mathbf{X}$ and $\mathbf{x}$ the reference (Lagrange) and current (Euler) position vectors of a material element, and if the transformation tensor $\mathbf{F}$ is defined as the Jacobian $\partial\mathbf{x}/\partial\mathbf{X}$, the distortion $\mathbf{U}$ is the gradient of the displacement field:

$$\mathbf{U} = \mathbf{F} - \mathbf{I} = \mathbf{grad}\,\mathbf{u}, \tag{10}$$

which implies that $\mathbf{U}$ is curl-free:

$$\mathbf{curl}\,\mathbf{U} = 0. \tag{11}$$

Eq.(11) is a necessary condition for the integrability of the distortion $\mathbf{U}$, commonly referred to as the compatibility condition for $\mathbf{U}$. Conversely, Eq.(11) is a sufficient condition for the existence of a single-valued continuous solution $\mathbf{u}$ of Eq.(10), up to a constant translation. Similarly, assuming that the distortion field is single-valued implies that the second-order distortion field $\mathbf{G} = \mathbf{grad}\,\mathbf{U}$ be curl-free:

$$\mathbf{curl}\,\mathbf{G} = 0. \tag{12}$$

Hence, Eq.(12) is a necessary condition for the existence of a single valued distortion field $\mathbf{U}$. It is also a sufficient condition for the existence of $\mathbf{U}$, up to a constant distortion. Eq.(9) implies that the rotation vector $\vec{\boldsymbol{\omega}}$ be divergence-free:

$$div\,\vec{\boldsymbol{\omega}} = 0. \tag{13}$$

Eq.(13) is known as the compatibility condition for $\vec{\boldsymbol{\omega}}$. The distortion $\mathbf{U}$ may be split into its symmetric part $\boldsymbol{\epsilon}$ (the strain tensor) and skew-symmetric part $\boldsymbol{\omega}$ (the spin or rotation tensor). Using the alternating rules (5,6), the latter is equivalent to the rotation vector $\vec{\boldsymbol{\omega}}$,

$$\vec{\boldsymbol{\omega}} = -\frac{1}{2}\,\boldsymbol{\omega} : \mathbf{X},\ \boldsymbol{\omega} = -\mathbf{X}.\vec{\boldsymbol{\omega}}. \tag{14}$$

The second-order curvature tensor $\boldsymbol{\kappa}$ is defined as:

$$\boldsymbol{\kappa} = \mathbf{grad}\,\vec{\boldsymbol{\omega}}. \tag{15}$$

Therefore, it is curl-free:

$$\mathbf{curl}\,\boldsymbol{\kappa} = 0. \tag{16}$$

Eq.(16) is a necessary condition for the integrability of $\boldsymbol{\kappa}$, referred to as the compatibility condition for the curvature tensor. Conversely, Eq.16 is a sufficient condition for the existence of a single-valued continuous solution $\vec{\boldsymbol{\omega}}$ of Eq.(15), up to a constant rotation. Note that $\boldsymbol{\kappa}$ is a deviatoric tensor, due to Eqs.(13,15), and that it may also read

$$\boldsymbol{\kappa} = -\frac{1}{2}\mathbf{X} : \mathbf{G}^{skew} \tag{17}$$

when expressed in terms of the skew-symmetric part (in the first two index positions) $\mathbf{G}^{skew}$ of $\mathbf{G}$. According to the alternating rules (7,8), $\mathbf{G}^{skew}$ can be identified with the third-order curvature tensor $\tilde{\boldsymbol{\kappa}}$:

$$\boldsymbol{\kappa} = -\frac{1}{2}\mathbf{X} : \tilde{\boldsymbol{\kappa}},\ \tilde{\boldsymbol{\kappa}} = -\mathbf{X}.\boldsymbol{\kappa}. \tag{18}$$

Hence, Eq.(16) may be converted into the third-order integrability condition:

$$\mathbf{curl}\,\tilde{\boldsymbol{\kappa}} = -\mathbf{X}.\mathbf{curl}\,\boldsymbol{\kappa} = 0. \tag{19}$$

Using the strain and curvature tensors $\boldsymbol{\epsilon}$ and $\boldsymbol{\kappa}$, the compatibility condition (11) also read:

$$\mathbf{curl}\,\boldsymbol{\epsilon} + tr(\boldsymbol{\kappa})\mathbf{I} - \boldsymbol{\kappa}^t = 0. \tag{20}$$

Transposing Eq.(20) and taking the curl of the transpose shows that $\boldsymbol{\epsilon}$ needs to satisfy the necessary condition:

$$\mathbf{curl}\,\mathbf{curl}^t\,\boldsymbol{\epsilon} = 0, \tag{21}$$

commonly referred to as Saint-Venant's compatibility condition. Splitting the second-order distortion into its symmetric, $\boldsymbol{\zeta}$, and skew-symmetric, $\tilde{\boldsymbol{\kappa}}$, parts (according to the first two index positions):

$$\mathbf{G} = \boldsymbol{\zeta} + \tilde{\boldsymbol{\kappa}}, \tag{22}$$

and using Eqs.(12,19,22) leads to an integrability condition on $\boldsymbol{\zeta}$:

$$\mathbf{curl}\,\boldsymbol{\zeta} = 0, \tag{23}$$

which guarantees that the strain tensor $\boldsymbol{\epsilon}$ can be found by integrating

$$\boldsymbol{\zeta} = \mathbf{grad}\,\boldsymbol{\epsilon}. \tag{24}$$

Assuming that the fields ($\boldsymbol{\zeta}$, $\boldsymbol{\kappa}$) are known and satisfy the conditions (19,23), one can find single-valued expressions for the fields $\boldsymbol{\epsilon}, \vec{\boldsymbol{\omega}}$ and $\mathbf{u}$ at any point $\mathbf{r}$ in the body. Indeed, upon integrating Eqs.(15,24), the expressions for $(\boldsymbol{\epsilon}, \vec{\boldsymbol{\omega}}, \mathbf{U})$ are found as:

$$\boldsymbol{\epsilon}(\mathbf{r}) = \boldsymbol{\epsilon}(\mathbf{r}_0) + \int_{\mathbf{r}_0}^{\mathbf{r}} \mathbf{d}\boldsymbol{\epsilon}' = \boldsymbol{\epsilon}(\mathbf{r}_0) + \int_{\mathbf{r}_0}^{\mathbf{r}} \boldsymbol{\zeta}'.\mathbf{dr}', \tag{25}$$

$$\vec{\boldsymbol{\omega}}(\mathbf{r}) = \vec{\boldsymbol{\omega}}(\mathbf{r}_0) + \int_{\mathbf{r}_0}^{\mathbf{r}} \mathbf{d}\vec{\boldsymbol{\omega}}' = \vec{\boldsymbol{\omega}}(\mathbf{r}_0) + \int_{\mathbf{r}_0}^{\mathbf{r}} \boldsymbol{\kappa}' \cdot \mathbf{dr}', \tag{26}$$

$$\mathbf{U}(\mathbf{r}) = \mathbf{U}(\mathbf{r}_0) + \int_{\mathbf{r}_0}^{\mathbf{r}} \mathbf{dU}' = \mathbf{U}(\mathbf{r}_0) + \int_{\mathbf{r}_0}^{\mathbf{r}} (\boldsymbol{\zeta}' - \mathbf{X}.\boldsymbol{\kappa}').\mathbf{dr}' \tag{27}$$

where $(\mathbf{r}, \mathbf{r}')$ denote position vectors, and $\mathbf{r}_0$ corresponds to some particular point where $(\boldsymbol{\epsilon}(\mathbf{r}_0), \vec{\boldsymbol{\omega}}(\mathbf{r}_0), \mathbf{U}(\mathbf{r}_0))$ are known. The displacement $\mathbf{u}$ is then found by integrating Eq.(10), which leads successively to:

$$\mathbf{u}(\mathbf{r}) = \mathbf{u}(\mathbf{r}_0) + \int_{\mathbf{r_0}}^{\mathbf{r}} \mathbf{U}' \cdot \mathbf{dr}' = \mathbf{u}(\mathbf{r}_0) + \int_{\mathbf{r_0}}^{\mathbf{r}} (\mathbf{U}(\mathbf{r}_0) + \int_{\mathbf{r_0}}^{\mathbf{r}'} (\boldsymbol{\zeta}" - \mathbf{X}.\boldsymbol{\kappa}").\mathbf{dr}").\mathbf{dr}', \tag{28}$$

$$\mathbf{u}(\mathbf{r}) = \mathbf{u}(\mathbf{r}_0) + \mathbf{U}(\mathbf{r}_0) \cdot (\mathbf{r} - \mathbf{r}_0) + \int_{\mathbf{r}_0}^{\mathbf{r}} (\int_{\mathbf{r}_0}^{\mathbf{r}'} \boldsymbol{\zeta}".\mathbf{dr}").\mathbf{dr}' + \int_{\mathbf{r}_0}^{\mathbf{r}} (\int_{\mathbf{r}_0}^{\mathbf{r}'} d\boldsymbol{\omega}").\mathbf{dr}', \tag{29}$$

$$\mathbf{u}(\mathbf{r}) = \mathbf{u}(\mathbf{r}_0) + \mathbf{U}(\mathbf{r}_0).(\mathbf{r} - \mathbf{r}_0) + \int_{\mathbf{r}_0}^{\mathbf{r}} (\int_{\mathbf{r}_0}^{\mathbf{r}'} \boldsymbol{\zeta}".\mathbf{dr}").\mathbf{dr}' + \int_{\mathbf{r}_0}^{\mathbf{r}} (\boldsymbol{\omega}(\mathbf{r}') - \boldsymbol{\omega}(\mathbf{r}_0)).\mathbf{dr}' \tag{30}$$

$$\mathbf{u}(\mathbf{r}) = \mathbf{u}(\mathbf{r}_0) + \boldsymbol{\epsilon}(\mathbf{r}_0).(\mathbf{r} - \mathbf{r}_0) + \int_{\mathbf{r}_0}^{\mathbf{r}} (\int_{\mathbf{r}_0}^{\mathbf{r}'} \boldsymbol{\zeta}".\mathbf{dr}").\mathbf{dr}' + \int_{\mathbf{r}_0}^{\mathbf{r}} \vec{\boldsymbol{\omega}}' \times \mathbf{dr}', \tag{31}$$

$$\begin{aligned} \mathbf{u}(\mathbf{r}) &= \mathbf{u}(\mathbf{r}_0) + \boldsymbol{\epsilon}(\mathbf{r}_0).(\mathbf{r} - \mathbf{r}_0) + \int_{\mathbf{r}_0}^{\mathbf{r}} (\int_{\mathbf{r}_0}^{\mathbf{r}'} \boldsymbol{\zeta}".\mathbf{dr}").\mathbf{dr}' + ... \\ ...+ &\int_{\mathbf{r}_0}^{\mathbf{r}} [-\mathbf{d}(\vec{\boldsymbol{\omega}}' \times (\mathbf{r} - \mathbf{r}')) + \mathbf{d}\vec{\boldsymbol{\omega}}' \times (\mathbf{r} - \mathbf{r}')], \end{aligned} \tag{32}$$

$$\mathbf{u}(\mathbf{r}) = \mathbf{u}(\mathbf{r}_0) + \mathbf{U}(\mathbf{r}_0).(\mathbf{r} - \mathbf{r}_0) + \int_{\mathbf{r}_0}^{\mathbf{r}} (\int_{\mathbf{r}_0}^{\mathbf{r}'} \boldsymbol{\zeta}".\mathbf{dr}").\mathbf{dr}' + \int_{\mathbf{r_0}}^{\mathbf{r}} (\boldsymbol{\kappa}'^t \times (\mathbf{r} - \mathbf{r}'))^t.\mathbf{dr}' \tag{33}$$

where it is assumed that $\mathbf{u}(\mathbf{r}_0)$ is known. By specializing Eqs.(25,26,33) to a closed circuit C starting and ending at point $\mathbf{r}_0$, and further using the Stokes theorem over C and the

surface S bounded by C, of unit normal $\mathbf{n}$, it is found that:

$$\oint_C \boldsymbol{\zeta} \cdot \mathbf{dr} = \int_S \mathbf{curl}\, \boldsymbol{\zeta}.\mathbf{n} dS = 0 \tag{34}$$

$$\oint_C \boldsymbol{\kappa} \cdot \mathbf{dr} = \int_S \mathbf{curl}\, \boldsymbol{\kappa}.\mathbf{n} dS = 0 \tag{35}$$

and, successively:

$$\oint_C [\boldsymbol{\epsilon} + (\boldsymbol{\kappa}^t \times (\mathbf{r_0} - \mathbf{r}))^t] \cdot \mathbf{dr} = \int_S \mathbf{curl}\, [\boldsymbol{\epsilon} + (\boldsymbol{\kappa}^t \times (\mathbf{r_0} - \mathbf{r}))^t] \cdot \mathbf{n} dS = ...$$

$$\int_S [\mathbf{curl}\, \boldsymbol{\epsilon} + ((\mathbf{curl}\, \boldsymbol{\kappa})^t \times (\mathbf{r}_0 - \mathbf{r}))^t + tr(\boldsymbol{\kappa})\mathbf{I} - \boldsymbol{\kappa}^t].\mathbf{n} dS = 0. \tag{36}$$

where the ' for the dummy variables is omitted in the integrals. The above compatibility conditions on the distortion, strain, rotation and second-order distortion ensure that continuity of the body is maintained along the deformation process. However, they may not be all satisfied by the elastic and plastic components of these quantities in the presence of crystal defects (dislocations and g-disclinations). The corresponding incompatibilities are now discussed.

3.2 Incompatibility in dislocation theory

In this Section, the symmetric, $(\boldsymbol{\zeta}_e, \boldsymbol{\zeta}_p)$, and skew-symmetric, $(\boldsymbol{\kappa}_e, \boldsymbol{\kappa}_p)$, parts of the elastic/plastic second-order distortion fields are assumed to be compatible. Hence, they satisfy the compatibility equations

$$\mathbf{curl}\, \tilde{\boldsymbol{\kappa}}_e = -\mathbf{X}.\mathbf{curl}\, \boldsymbol{\kappa}_e = 0, \tag{37}$$

$$\mathbf{curl}\, \tilde{\boldsymbol{\kappa}}_p = -\mathbf{X}.\mathbf{curl}\, \boldsymbol{\kappa}_p = 0, \tag{38}$$

$$\mathbf{curl}\, \boldsymbol{\zeta}_e = 0, \tag{39}$$

$$\mathbf{curl}\, \boldsymbol{\zeta}_p = 0, \tag{40}$$

in analogy with Eqs.(19,23), which concern the total second-order distortion field. Therefore the elastic strain and rotation fields are single-valued at any point in the body and, in analogy with Eqs.(25,26), they can be computed according to

$$\boldsymbol{\epsilon}_e(\mathbf{r}) = \boldsymbol{\epsilon}_e(\mathbf{r}_0) + \int_{\mathbf{r}_0}^{\mathbf{r}} \mathbf{d}\boldsymbol{\epsilon}'_e = \boldsymbol{\epsilon}_e(\mathbf{r}_0) + \int_{\mathbf{r}_0}^{\mathbf{r}} \boldsymbol{\zeta}'_e.\mathbf{dr}', \tag{41}$$

$$\vec{\boldsymbol{\omega}}_e(\mathbf{r}) = \vec{\boldsymbol{\omega}}_e(\mathbf{r}_0) + \int_{\mathbf{r}_0}^{\mathbf{r}} \mathbf{d}\vec{\boldsymbol{\omega}}'_e = \vec{\boldsymbol{\omega}}_e(\mathbf{r}_0) + \int_{\mathbf{r}_0}^{\mathbf{r}} \boldsymbol{\kappa}'_e \cdot \mathbf{dr}', \tag{42}$$

with similar relations for their plastic counterparts. This is the situation met in dislocation theory [Acharya, 2001]. Incompatibility is restricted to the elastic and plastic

distortions $(\mathbf{U}_e, \mathbf{U}_p)$. The elastic/plastic vector fields $(\mathbf{u}_e, \mathbf{u}_p)$ may become multi-valued, and constant discontinuities ($[\![\mathbf{u}_e]\!]$,$[\![\mathbf{u}_p]\!]$) may be found across bounded surfaces by integrating the elastic/plastic displacements along closed circuits known as Burgers circuits. Computing the elastic displacement in the manner of Eq.(36) leads to:

$$\int_S (\mathbf{curl}\,\boldsymbol{\epsilon}_e + tr(\boldsymbol{\kappa}_e)\mathbf{I} - \boldsymbol{\kappa}_e{}^t).\mathbf{n}dS = \int_S \boldsymbol{\alpha}.\mathbf{n}dS = [\![\mathbf{u}_e]\!] = \mathbf{b}, \tag{43}$$

where $\mathbf{b}$ is defined as the Burgers vector, and $\boldsymbol{\alpha}$ is Nye's dislocation density tensor

$$\boldsymbol{\alpha} = \mathbf{curl}\,\boldsymbol{\epsilon}_e + tr(\boldsymbol{\kappa}_e)\mathbf{I} - \boldsymbol{\kappa}_e{}^t = \mathbf{curl}\,\mathbf{U}_e. \tag{44}$$

Due to continuity of the body: $[\![\mathbf{u}_p]\!] = -[\![\mathbf{u}_e]\!]$, and $\boldsymbol{\alpha}$ can be similarly characterized by the relation:

$$\boldsymbol{\alpha} = -(\mathbf{curl}\,\boldsymbol{\epsilon}_p + tr(\boldsymbol{\kappa}_p)\mathbf{I} - \boldsymbol{\kappa}_p{}^t) = -\mathbf{curl}\,\mathbf{U}_p. \tag{45}$$

The comparison with the compatibility equation (20) further confers their meaning to Eqs.(44,45). Note that, using Eq.(4), $\boldsymbol{\alpha}$ may also read:

$$\boldsymbol{\alpha} = -\mathbf{G}_e : \mathbf{X} = -\boldsymbol{\zeta}_e : \mathbf{X} - \tilde{\boldsymbol{\kappa}}_e : \mathbf{X} = -\boldsymbol{\zeta}_e : \mathbf{X} + tr(\boldsymbol{\kappa}_e)\mathbf{I} - \boldsymbol{\kappa}_e{}^t, \tag{46}$$

in terms of the second-order elastic distortion $\mathbf{G}_e$ or, using the plastic counterparts:

$$\boldsymbol{\alpha} = \mathbf{G}_p : \mathbf{X} = \boldsymbol{\zeta}_p : \mathbf{X} + \tilde{\boldsymbol{\kappa}}_p : \mathbf{X} = \boldsymbol{\zeta}_p : \mathbf{X} - tr(\boldsymbol{\kappa}_p)\mathbf{I} + \boldsymbol{\kappa}_p{}^t, \tag{47}$$

expressions that will become useful below, when $(\mathbf{G}_e, \mathbf{G}_p)$ cease to be compatible. Taking the trace of Eqs.(44,45), we also find the compatibility conditions for the elastic/plastic rotations:

$$div(\vec{\boldsymbol{\omega}}_e) = -div(\vec{\boldsymbol{\omega}}_p) = \frac{1}{2}tr(\boldsymbol{\alpha}) \tag{48}$$

to be viewed in parallel with Eq.(13). Motivated by Saint-Venant's compatibility condition (21), we transpose Eqs.(44,45), take the curl of the latter and further re-arrange to obtain the incompatibility tensor $\boldsymbol{\eta}$:

$$\boldsymbol{\eta} = (\mathbf{curl}\,\mathbf{curl}^t\,\boldsymbol{\epsilon}_e)^{sym} = -(\mathbf{curl}\,\mathbf{curl}^t\,\boldsymbol{\epsilon}_p)^{sym} = (\mathbf{curl}\,(\boldsymbol{\alpha}^t))^{sym}. \tag{49}$$

In the absence of dislocations, $\boldsymbol{\eta} = 0$ and Eq.(49) reduces to Saint-Venant's compatibility equation.

3.3 Incompatibility in dislocation/standard disclination theory

We now assume that, in addition to the incompatibility of the elastic/plastic distortion, the skew-symmetric part of the elastic/plastic second-order distortion, *i.e.* the third-order elastic/plastic curvature tensor $(\tilde{\boldsymbol{\kappa}}_e, \tilde{\boldsymbol{\kappa}}_p)$, is incompatible, but that its symmetric part

retains compatibility. Eqs.(39,40) are therefore still satisfied, and the elastic strain can still be computed at any point in the body according to Eq.(41). In contrast, discontinuities ($[\![\vec{\boldsymbol{\omega}}_e]\!]$,$[\![\vec{\boldsymbol{\omega}}_p]\!]$) may be found in integrating the elastic/plastic rotations along closed circuits, in addition to translations. This is the situation met in the field theory of disclinations [deWit, 1970; Fressengeas et al., 2011]. Doing so in the manner of Eq.(35) leads to the angular closure defect $\boldsymbol{\Omega}$ known as the Frank vector:

$$\boldsymbol{\Omega} = [\![\vec{\boldsymbol{\omega}}_e]\!] = \oint_C \boldsymbol{\kappa}_e.\mathbf{dr} = \int_S \mathbf{curl}\,\boldsymbol{\kappa}_e.\mathbf{n}dS. \tag{50}$$

A non-vanishing tensor field $\boldsymbol{\theta}$ referred to as the disclination density tensor field then exists, such that:

$$\mathbf{curl}\,\boldsymbol{\kappa}_e = -\mathbf{curl}\,\boldsymbol{\kappa}_p = \boldsymbol{\theta} \tag{51}$$

and

$$\boldsymbol{\Omega} = \int_S \boldsymbol{\theta}.\mathbf{n}dS. \tag{52}$$

Calculating the elastic displacement along closed circuits in the manner of Eq.(36) leads to the discontinuity $[\![\mathbf{u}_e]\!]$:

$$[\![\mathbf{u}_e]\!] \;=\; \oint_C [\boldsymbol{\epsilon}_e + (\boldsymbol{\kappa}_e^t \times (\mathbf{r_0} - \mathbf{r}))^t] \cdot \mathbf{dr}. \tag{53}$$

Substituting Frank's vector $\boldsymbol{\Omega}$ in Eq.(53), we find:

$$[\![\mathbf{u}_e]\!] = \oint_C [\boldsymbol{\epsilon}_e - (\boldsymbol{\kappa}_e^t \times \mathbf{r})^t].\mathbf{dr} + \boldsymbol{\Omega} \times \mathbf{r}_0. \tag{54}$$

We now define the displacement closure defect $\mathbf{b}$ as:

$$\mathbf{b} = \oint_C [\boldsymbol{\epsilon}_e - (\boldsymbol{\kappa}_e^t \times \mathbf{r})^t].\mathbf{dr} \tag{55}$$

and obtain the displacement discontinuity $[\![\mathbf{u}_e]\!]$:

$$[\![\mathbf{u}_e]\!] = \mathbf{b} + \boldsymbol{\Omega} \times \mathbf{r}_0. \tag{56}$$

$[\![\mathbf{u}_e]\!]$ may be seen as deriving from the motion of a rigid body submitted to the rotation $\boldsymbol{\Omega}$ and translation $\mathbf{b}$, as in Weingarten's theorem [Weingarten, 1901]. Using the Stokes theorem in Eq.(55), $\mathbf{b}$ can also be written as:

$$\mathbf{b} = \int_S \mathbf{curl}\,[\boldsymbol{\epsilon}_e - (\boldsymbol{\kappa}_e^t \times \mathbf{r})^t].\mathbf{n}dS = \int_S [\mathbf{curl}\,\boldsymbol{\epsilon}_e - ((\mathbf{curl}\,\boldsymbol{\kappa}_e)^t \times \mathbf{r})^t + tr(\boldsymbol{\kappa}_e)\mathbf{I} - \boldsymbol{\kappa}_e^t].\mathbf{n}dS. \tag{57}$$

Using Eqs.(44,51) to substitute the dislocation and disclination density tensors $(\boldsymbol{\alpha}, \boldsymbol{\theta})$ in Eq.(57), it is found that the Burgers vector derives from the latter through the relation:

$$\mathbf{b} = \int_S (\boldsymbol{\alpha} - (\boldsymbol{\theta}^t \times \mathbf{r})^t).\mathbf{n} dS. \tag{58}$$

In the presence of dislocations and disclinations, the incompatibility tensor $\boldsymbol{\eta}$ computed by taking the curl of the transpose of Eqs.(44,45), just as in the previous section, is now defined as:

$$\boldsymbol{\eta} = (\mathbf{curl}\,\mathbf{curl}^t\,\boldsymbol{\epsilon}_e - \mathbf{curl}\,\boldsymbol{\kappa}_e)^{sym} = (\mathbf{curl}\,(\boldsymbol{\alpha}^t))^{sym}. \tag{59}$$

3.4 Incompatibility in dislocation/g-disclination theory

We now assume incompatibility of both the symmetric and skew-symmetric parts of the elastic/plastic second-order distortion. In addition to discontinuities of the elastic/plastic displacement and rotation fields, an arbitrary discontinuity of the elastic/plastic strain tensors ($[\![\boldsymbol{\epsilon}_e]\!]$,$[\![\boldsymbol{\epsilon}_p]\!]$) may now be expected in integrating the elastic/plastic symmetric second-order distortions along closed circuits. This is the situation discussed in the field theory of generalized disclinations of Acharya and Fressengeas [2012, 2015]. Performing such a calculation for the elastic symmetric second-order distortion $\boldsymbol{\zeta}_e$ by setting $\mathbf{r} = \mathbf{r}_0$ in Eq.(41) leads to the elastic strain closure defect tensor $\boldsymbol{\Xi}$:

$$\boldsymbol{\Xi} = [\![\boldsymbol{\epsilon}_e]\!] = \oint_C \boldsymbol{\zeta}_e.\mathbf{dr} = \int_S \mathbf{curl}\,\boldsymbol{\zeta}_e.\mathbf{n} dS. \tag{60}$$

A non-vanishing third-order tensor field $\boldsymbol{\xi}$ then exists such that:

$$\mathbf{curl}\,\boldsymbol{\zeta}_e = -\mathbf{curl}\,\boldsymbol{\zeta}_p = \boldsymbol{\xi} \tag{61}$$

and

$$\boldsymbol{\Xi} = \int_S \boldsymbol{\xi}.\mathbf{n} dS. \tag{62}$$

Since the elastic/plastic rotation vectors also encounter discontinuities, Eqs.(50-52) still hold, and we see from Eq.(51) that

$$\mathbf{curl}\,\tilde{\boldsymbol{\kappa}}_e = -\mathbf{X}.\mathbf{curl}\,\boldsymbol{\kappa}_e = -\mathbf{curl}\,\tilde{\boldsymbol{\kappa}}_p = \mathbf{X}.\mathbf{curl}\,\boldsymbol{\kappa}_p = -\mathbf{X}.\boldsymbol{\theta}. \tag{63}$$

Therefore, we may write:

$$\mathbf{curl}\,\mathbf{G}_e = \mathbf{curl}\,(\boldsymbol{\zeta}_e + \tilde{\boldsymbol{\kappa}}_e) = \boldsymbol{\xi} - \mathbf{X}.\boldsymbol{\theta} = \boldsymbol{\pi} = -\mathbf{curl}\,\mathbf{G}_p. \tag{64}$$

Eq.(64) defines the g-disclination density tensor $\boldsymbol{\pi}$, which essentially reduces to the standard disclination density tensor $\boldsymbol{\theta}$ in the absence of an elastic/plastic strain discontinuity

($\boldsymbol{\xi} = 0$). Integrating $\boldsymbol{\pi}$ over surface S yields the discontinuity $\mathbf{\Pi} = [\![\mathbf{U}_e]\!]$ of the elastic distortion, which can also be obtained from the integration of the elastic second-order distortion along curve C through the Stokes theorem:

$$\mathbf{\Pi} = [\![\mathbf{U}_e]\!] = \int_S \boldsymbol{\pi}.\mathbf{n} dS = \int_S \mathbf{curl}\, \mathbf{G}_e.\mathbf{n} dS = \oint_C \mathbf{G}_e.\mathbf{dr}. \tag{65}$$

The discontinuity $[\![\mathbf{u}_e]\!]$ of the elastic displacement along the closed circuit C is obtained by setting $\mathbf{r} = \mathbf{r}_0$ in the elastic analog of Eq.(33):

$$[\![\mathbf{u}_e]\!] = \oint_C (\int_{\mathbf{r}_0}^{\mathbf{r}'} \boldsymbol{\zeta}_e".\mathbf{dr}").\mathbf{dr}' + \oint_C ({\boldsymbol{\kappa}'_e}^t \times (\mathbf{r}_0 - \mathbf{r}'))^t.\mathbf{dr}'. \tag{66}$$

The resulting Burgers vector is still given by Eq.(58), but with the dislocation density tensor reading $\boldsymbol{\alpha} = -\mathbf{G}_e : \mathbf{X}$, as in Eq.(46). In defining the incompatibility tensor $\boldsymbol{\eta}$, Eqs.(46,49) also suggest that the adequate generalization of Eq.(59) in the context of g-disclinations is:

$$\boldsymbol{\eta} = (\mathbf{curl}\, (-\mathbf{G}_e : \mathbf{X})^t)^{sym} = (\mathbf{curl}\, \boldsymbol{\alpha}^t)^{sym}. \tag{67}$$

Finally, taking the divergence of $\boldsymbol{\pi}$ in Eq.(64) leads to the continuity equation

$$\mathbf{div}\, \boldsymbol{\pi} = 0, \tag{68}$$

whose meaning is that g-disclination lines do not end in the body. Taking similarly the divergence of $\boldsymbol{\alpha}$ in Eq.(46) and using Eq.(64) leads to

$$\alpha_{ij,j} = -e_{klj} G^e_{ikl,j} = e_{kjl} G^e_{ikl,j} = (\mathbf{curl}\, \mathbf{G}_e)_{ikk} = \pi_{ikk}, \tag{69}$$

and therefore to

$$\mathbf{div}\, \boldsymbol{\alpha} = \boldsymbol{\pi} : \mathbf{I} \tag{70}$$

in intrinsic form. This continuity equation implies geometric interactions between dislocations and g-disclinations and further suggests that dislocation lines may end in the body at g-disclinations.

4 Transport

The dislocation, standard disclination and generalized disclination density fields $(\boldsymbol{\alpha}, \boldsymbol{\theta})$ and $\boldsymbol{\xi}$ are aeral densities of defect lines carrying a topological content, respectively $(\mathbf{b}, \mathbf{\Omega})$ and Ξ. We now assume that they have associated velocity fields, $(\mathbf{V}_\alpha, \mathbf{V}_\theta)$ and $\mathbf{V}_\xi$ with respect to the material. At sufficiently small resolution length scales, $(\boldsymbol{\alpha}, \boldsymbol{\theta}, \boldsymbol{\xi})$ represent individual defects, and the corresponding velocity fields reflect the motions of the defects' cores. At larger length scales, they may represent the averaged velocity of a larger

ensemble of defects. Conservation laws for their topological content follow from the kinematics of defect line fluxes into a patch [Acharya, 2011]. For the symmetric part of the g-disclination density, the point-wise form of the conservation law for the elastic/plastic strain tensor discontinuity $\boldsymbol{\Xi}$ is:

$$\dot{\boldsymbol{\xi}} + \mathbf{curl}\,(\boldsymbol{\xi} \times \mathbf{V}_\xi) = 0 \tag{71}$$

in the absence of defect nucleation in the patch. Independently, the time derivative of Eq.(61) implies

$$\dot{\boldsymbol{\xi}} + \mathbf{curl}\,\dot{\boldsymbol{\zeta}}_p = 0, \tag{72}$$

and it follows from the two previous statements that

$$\dot{\boldsymbol{\zeta}}_p = \boldsymbol{\xi} \times \mathbf{V}_\xi + \mathbf{grad}\,\dot{\boldsymbol{\epsilon}}_s, \tag{73}$$

where $\dot{\boldsymbol{\epsilon}}_s$ is a second-order tensor with dimension and symmetry of a strain-rate. Further, $\mathbf{grad}\,\dot{\boldsymbol{\epsilon}}_s$ belongs to the symmetric part of the anelastic second-order distortion rate $\dot{\boldsymbol{\zeta}}_p$, but does not contribute to its incompatibility. As such, $\dot{\boldsymbol{\epsilon}}_s$ reflects a change in $\dot{\boldsymbol{\zeta}}_p$ that results from a compatible deformation of the body not involving the motion of disclinations. In a manner similar to Eq.(71), the point-wise form for the conservation of the Frank vector $\boldsymbol{\Omega}$ is:

$$\dot{\boldsymbol{\theta}} + \mathbf{curl}\,(\boldsymbol{\theta} \times \mathbf{V}_\theta) = 0 \tag{74}$$

in the absence of sources. Independently, the time derivative of Eq.(63) implies

$$\dot{\boldsymbol{\theta}} + \mathbf{curl}\,\dot{\boldsymbol{\kappa}}_p = 0, \tag{75}$$

and it follows from the Eqs.(74,75) that

$$\dot{\boldsymbol{\kappa}}_p = \boldsymbol{\theta} \times \mathbf{V}_\theta + \dot{\boldsymbol{\kappa}}_s, \tag{76}$$

where $\dot{\boldsymbol{\kappa}}_s$ is a plastic curvature rate tensor potentially reflecting a change in $\dot{\boldsymbol{\kappa}}_p$ that arises from a compatible transformation of the body not involving the motion of g-disclinations. Alternating Eq.(75) in the form

$$\mathbf{X}.\dot{\boldsymbol{\theta}} = -\mathbf{X}.\mathbf{curl}\,\dot{\boldsymbol{\kappa}}_p \tag{77}$$

and combining Eqs.(72,73,76,77), we find

$$\dot{\boldsymbol{\pi}} = -\mathbf{curl}\,(\boldsymbol{\xi} \times \mathbf{V}_\xi + \mathbf{grad}\,\dot{\boldsymbol{\epsilon}}_s - \mathbf{X}.(\boldsymbol{\theta} \times \mathbf{V}_\theta + \dot{\boldsymbol{\kappa}}_s)). \tag{78}$$

By generically denoting both $\mathbf{V}_\theta$ and $\mathbf{V}_\xi$ as $\mathbf{V}_\pi$, *i.e.* as the velocity of a g-disclination density, it is seen that the above relation is also:

$$\dot{\boldsymbol{\pi}} = -\mathbf{curl}\,((\boldsymbol{\xi} - \mathbf{X}.\boldsymbol{\theta}) \times \mathbf{V}_\pi + \mathbf{grad}\,\dot{\boldsymbol{\epsilon}}_s - \mathbf{X}.\dot{\boldsymbol{\kappa}}_s) = -\mathbf{curl}\,(\boldsymbol{\pi} \times \mathbf{V}_\pi + \mathbf{grad}\,\dot{\boldsymbol{\epsilon}}_s + \dot{\tilde{\boldsymbol{\kappa}}}_s), \tag{79}$$

where the third-order curvature rate tensor $\dot{\boldsymbol{\kappa}}_s$ is the gradient of a skew-symmetric rotation rate tensor $\dot{\boldsymbol{\omega}}_s$: $\dot{\boldsymbol{\kappa}}_s = \mathbf{grad}\,\dot{\boldsymbol{\omega}}_s$. Eq.(79) appears as the transport equation for the g-disclination density field $\boldsymbol{\pi}$. Taking the time derivative of Eq.64, and accounting for Eq.(73), we find from Eq.(79):

$$\dot{\boldsymbol{\pi}} + \mathbf{curl}\,\dot{\mathbf{G}}_p = 0, \dot{\mathbf{G}}_p = \boldsymbol{\pi} \times \mathbf{V}_\pi + \mathbf{grad}\,\dot{\mathbf{U}}_s, \tag{80}$$

where $\dot{\mathbf{U}}_s = \dot{\boldsymbol{\epsilon}}_s + \dot{\boldsymbol{\omega}}_s$ is a compatible anelastic distortion rate not contributing to the incompatibility of $\dot{\mathbf{G}}_p$ and independent of the motion of g-disclinations. $\dot{\mathbf{U}}_s$ may be split into the plastic distortion rate $\dot{\mathbf{U}}_p$ resulting from the motion of dislocations, as defined below in Eq.(85), and possibly a term $\dot{\mathbf{Z}}_s$ independent of the motion of dislocations and g-disclinations:

$$\dot{\mathbf{G}}_p = \boldsymbol{\pi} \times \mathbf{V}_\pi + \mathbf{grad}\,\dot{\mathbf{U}}_p + \mathbf{grad}\,\dot{\mathbf{Z}}_s. \tag{81}$$

At a sufficiently large resolution length scale, $\dot{\mathbf{Z}}_s$ may be identified with the compatible plastic distortion rate $\mathbf{L}_p$ produced by the motion of the so-called "statistical dislocations". We may assume $\dot{\mathbf{Z}}_s = 0$ when the resolution length scale is sufficiently small. Note that a consequence of Eqs.(71,75,80) is that

$$\mathbf{div}\,\dot{\boldsymbol{\xi}} = \mathbf{div}\,\dot{\boldsymbol{\theta}} = 0,\ \mathbf{div}\,\dot{\boldsymbol{\pi}} = 0, \tag{82}$$

which has the physical meaning that g-disclination lines do not terminate inside the body.

We now turn to the conservation equation for the Burgers vector and transport equation for the dislocation densities. Taking the time derivative of Eq.(47), we find the rate of dislocation density as:

$$\dot{\boldsymbol{\alpha}} = \dot{\mathbf{G}}_p : \mathbf{X}. \tag{83}$$

Decomposing the anelastic second-order distortion rate into its compatible and incompatible parts, and taking advantage of the identity (4), we note from Eq.(83) that

$$\dot{\boldsymbol{\alpha}} - \dot{\mathbf{G}}_p^{\perp} : \mathbf{X} = \dot{\mathbf{G}}_p^{\parallel} : \mathbf{X} = -\mathbf{curl}\,\dot{\mathbf{U}}_p. \tag{84}$$

From the kinematics of the flux of dislocation lines moving into a patch through its bounding curve, we write:

$$\dot{\mathbf{U}}_p \ = \ \boldsymbol{\alpha} \times \mathbf{V}_\alpha \tag{85}$$

to finally obtain:

$$\dot{\boldsymbol{\alpha}} = -\mathbf{curl}\,(\boldsymbol{\alpha} \times \mathbf{V}_\alpha) + \dot{\mathbf{G}}_p^{\perp} : \mathbf{X} = -\mathbf{curl}\,(\boldsymbol{\alpha} \times \mathbf{V}_\alpha) + \mathbf{s}_\alpha. \tag{86}$$

Note that we did not include any additional gradient term in Eq.(85), owing to the assumed smallness of the resolution length scale. Here $\mathbf{s}_\alpha$ represents a source of dislocations arising from the motion of g-disclinations. Thus, dislocation generation may be predicted from g-disclination motion on the basis of Eq.(86). Indeed, detailed mechanisms for the multiplication of dislocations during martensitic transformation were recently uncovered in Transmission Electron Micoscopy observations of Ni-Ti single crystals [Simon et al., 2010].

5 Equilibrium equations and boundary conditions

In the second-order theory being developed here, the virtual power of internal forces P_i is assumed to be a function of the strain rate and second-order distortion rate tensor fields $(\dot{\boldsymbol{\epsilon}}, \dot{\mathbf{G}})$ in order to account for the kinematics of the dislocations and g-disclinations, and of their work-conjugate fields $(\mathbf{T}^{sym}, \mathbf{M})$, respectively the symmetric stress tensor and hyper-stress tensor fields:

$$P_i = -\int_V (\dot{\boldsymbol{\epsilon}} : \mathbf{T}^{sym} + \dot{\mathbf{G}} \vdots \mathbf{M}) dv. \tag{87}$$

Because it is symmetric, the strain rate tensor extracts the symmetric part of the stress tensor $\mathbf{T}$ but, although it is not involved in Eq.(87), the skew-symmetric stress tensor $\mathbf{T}^{skew}$ is expected to play a role in the balance of momentum in the following. Splitting the second-order distortion rate and hyper-stress tensors into their symmetric and skew-symmetric parts leads to

$$P_i = -\int_V (\dot{\boldsymbol{\epsilon}} : \mathbf{T}^{sym} + \dot{\mathbf{G}}^{skew} \vdots \mathbf{M}^{skew} + \dot{\mathbf{G}}^{sym} \vdots \mathbf{M}^{sym}) dv, \tag{88}$$

where the symmetric and skew-symmetric tensors extract respectively their dual symmetric and skew-symmetric counterparts in the inner products. Substituting the second-order curvature tensor $\boldsymbol{\kappa}$ for the skew-symmetric second-order distortion $\mathbf{G}^{skew}$ (see Eq.(18)) equivalently leads to the alternative expression of P_i:

$$P_i = -\int_V (\dot{\boldsymbol{\epsilon}} : \mathbf{T}^{sym} + \dot{\boldsymbol{\kappa}} : \tilde{\mathbf{M}} + \dot{\mathbf{G}}^{sym} \vdots \mathbf{M}^{sym}) dv \tag{89}$$

where $\tilde{\mathbf{M}}$ is the couple-stress tensor, related to the skew-symmetric part, $\mathbf{M}^{skew}$, of the hyper-stress tensor through the relations

$$\mathbf{M}^{skew} = -\mathbf{X}.\tilde{\mathbf{M}} \; ; \; \tilde{\mathbf{M}} = -\frac{1}{2}\mathbf{X} : \mathbf{M}^{skew}. \tag{90}$$

In any body occupying the volume V with boundary ∂V having outward unit normal field $\mathbf{n}$, the external power supplied to the body at any given time is expressed as:

$$P_e = \int_{\partial V} (\dot{\mathbf{u}}.\mathbf{t} + \dot{\mathbf{U}} : \boldsymbol{\Lambda}) dS, \tag{91}$$

where $\mathbf{t}$ and $\boldsymbol{\Lambda}$ are respectively the traction vector and second-order hyper-traction tensor applied to the external surface of the body, and where the volumetric densities of loads and inertial forces have been ignored for the sake of simplicity. The boundary conditions on ∂V are:

$$\mathbf{t} = (\mathbf{T} - \mathbf{div}\, \mathbf{M}^{sym}).\mathbf{n} \tag{92}$$

$$\boldsymbol{\Lambda} = \mathbf{M}.\mathbf{n}. \tag{93}$$

As a consequence, Eq.(91) becomes

$$P_e = \int_{\partial V} (\dot{\mathbf{u}}.(\mathbf{T} - \mathbf{div}\,\mathbf{M}^{sym}) + \dot{\mathbf{U}} : \mathbf{M}).\mathbf{n} dS, \tag{94}$$

which can be transformed into the volumetric integral

$$P_e = \int_V \mathbf{div}\,(\dot{\mathbf{u}}.(\mathbf{T} - \mathbf{div}\,\mathbf{M}^{sym}) + \dot{\mathbf{U}} : \mathbf{M}) dv \tag{95}$$

by invoking the divergence theorem. Developing the divergence, Eq.(95) can be further written as

$$P_e = \int_V (\dot{\mathbf{u}}.\mathbf{div}\,(\mathbf{T} - \mathbf{div}\,\mathbf{M}^{sym}) + \dot{\mathbf{U}} : (\mathbf{T} - \mathbf{div}\,\mathbf{M}^{sym}) + \dot{\mathbf{U}} : \mathbf{div}\,\mathbf{M} + \dot{\mathbf{G}} \vdots \mathbf{M}) dv, \tag{96}$$

or:

$$P_e = \int_V (\dot{\mathbf{u}}.\mathbf{div}\,(\mathbf{T} - \mathbf{div}\,\mathbf{M}^{sym}) + \dot{\boldsymbol{\epsilon}} : \mathbf{T}^{sym} + \dot{\boldsymbol{\omega}} : (\mathbf{T}^{skew} + \mathbf{div}\,\mathbf{M}^{skew}) + \dot{\mathbf{G}} \vdots \mathbf{M}) dv. \tag{97}$$

Using relations (87,97) in the application of the principle of virtual work: $P_e + P_i = 0$ for any differentiable virtual displacement field over the body yields the equations

$$\mathbf{div}\,(\mathbf{T} - \mathbf{div}\,\mathbf{M}^{sym}) = 0 \tag{98}$$

$$\mathbf{T}^{skew} + \mathbf{div}\,\mathbf{M}^{skew} = 0. \tag{99}$$

Eqs.(98,99) are the pointwise equilibrium equations of the body. They are consistent with the postulated internal energy density (87) and the boundary conditions (92,93). By combining these two equations, it is found that the following form of Eq.(98) is equally valid:

$$\mathbf{div}\,(\mathbf{T}^{sym} - \mathbf{div}\,\mathbf{M}) = 0. \tag{100}$$

Using relation (90) to substitute the couple-stress tensor $\tilde{\mathbf{M}}$ for $\mathbf{M}^{skew}$ in Eq.(99) leads equivalently to:

$$\mathbf{div}\,\tilde{\mathbf{M}} - \mathbf{X} : \mathbf{T} = 0, \tag{101}$$

which is the conventional balance equation for the moment of momentum in terms of stresses and couple-stresses. It is instructive to compare the rate of internal work (87-89), the boundary conditions (92,93) and balance equations (98,99) or (99,100) in the present theory with those introduced by Mindlin [1965] in the context of a compatible strain-gradient theory:

$$P_i = -\int_V (\dot{\boldsymbol{\epsilon}} : \mathbf{T}^{sym} + \dot{\mathbf{G}}^{sym} \vdots \mathbf{M}^{sym}) dv \tag{102}$$

$$0 = \mathbf{div}\,(\mathbf{T}^{sym} - \mathbf{div}\,\mathbf{M}^{sym}) \tag{103}$$

$$\mathbf{t} = (\mathbf{T}^{sym} - \mathbf{div}\,\mathbf{M}^{sym}).\mathbf{n}\, on\, \partial V \tag{104}$$

$$\boldsymbol{\Lambda} = \mathbf{M}^{sym}.\mathbf{n}\, on\, \partial V. \tag{105}$$

It is seen from the comparison that Mindlin's strain-gradient theory does not involve the skew-symmetric components of the stress and hyper-stress tensors. As a result, the moment of momentum equation (101) becomes irrelevant. In the present incompatible context with second-order crystal defects, using Eqs.(102-105) would have prevented consistent treatment of equilibrium in the presence of standard disclinations. A complementary comparison with the compatible couple-stress theory of Mindlin and Tiersten [1962] is also in order. In that paper, the skew-symmetric parts of the stress and hyper-stress tensors are considered, the latter being reducible to the couple-stress tensor as mentioned above, but the symmetric part of the hyper-stress tensor is not involved: $\mathbf{M}^{sym} = 0$. Since

$$\mathbf{div}\,\mathbf{div}\,\mathbf{M}^{skew} = -\frac{1}{2}\mathbf{curl}\,\mathbf{div}\,\tilde{\mathbf{M}}, \tag{106}$$

we then find from Eq.(100) that

$$\mathbf{div}\,\mathbf{T}^{sym} + \frac{1}{2}\mathbf{curl}\,\mathbf{div}\,\tilde{\mathbf{M}} = 0. \tag{107}$$

This is the balance equation shown in Mindlin and Tiersten [1962]. Therefore, the involvement of the symmetric part of the hyper-stress tensor in the present analysis amounts to complementarily generalizing the compatible couple-stress theory of Mindlin and Tiersten [1962] and the strain-gradient theory of Mindlin [1965] into a second-order distortion theory of incompatible media. The present theory may also be seen as an extension of the gradient theory discussed in Mindlin and Eshel [1968] to incompatible media.

Note that the external loading may be restricted by demanding that the hyper-traction tensors $\mathbf{\Lambda}^{sym}$ be self-balanced on the boundary ∂V, independently of the tractions $\mathbf{t}$ and skew-symmetric hyper-tractions $\mathbf{\Lambda}^{skew}$:

$$\int_{\partial V} \mathbf{\Lambda}^{sym} dS = \int_{\partial V} \mathbf{M}^{sym}.\mathbf{n} dS = 0. \tag{108}$$

From the divergence theorem, Eq.(108) implies that the symmetric part of the hyper-stress tensor is divergence-free in V:

$$\mathbf{div}\,\mathbf{M}^{sym} = 0. \tag{109}$$

Therefore, appending the Mindlin-Tiersten balance equation (107) with the self-balance equation of $\mathbf{M}^{sym}$ (109) provides a set of equations equivalent to the full Mindlin-Eshel system (99,100). This property was used in [Acharya and Fressengeas, 2015] to restrict the formulation to a couple-stress theory. It is further illustrated in Section 8.1. Clearly, there is no such equivalence between the Mindlin-Tiersten and Mindlin-Eshel frameworks in the absence of the constraints (108,109), which are not imposed here. Elastic constitutive relations for the symmetric stress tensor and hyper-stress tensor, and driving forces for the dissipative motion of dislocations and g-disclinations are now looked for by following thermodynamic arguments first presented by Coleman and Gurtin [1967].

6 Constitutive relations

The mechanical power dissipation is defined as the difference between the power of external loads applied to the body and the rate of free energy stored in the body:

$$D = \int_{\partial V} (\dot{\mathbf{u}}.\mathbf{t} + \dot{\mathbf{U}} : \mathbf{\Lambda}) dS - \int_V \dot{\psi} dv. \tag{110}$$

According to the second law of thermodynamics, D is non-negative in all dynamic processes, and vanishes only in purely elastic reversible processes. From the previous Section, it is readily seen that D can also be expressed as the volumetric integral:

$$D = \int_V (\dot{\boldsymbol{\epsilon}} : \mathbf{T}^{sym} + \dot{\mathbf{G}} \vdots \mathbf{M}) dv - \int_V \dot{\psi} dv. \tag{111}$$

or, in terms of the second-order curvature tensor $\boldsymbol{\kappa}$ and couple-stress tensor $\tilde{\mathbf{M}}$:

$$D = \int_V (\dot{\boldsymbol{\epsilon}} : \mathbf{T}^{sym} + \dot{\boldsymbol{\kappa}} : \tilde{\mathbf{M}}^{dev} + \dot{\mathbf{G}}^{sym} \vdots \mathbf{M}^{sym}) dv - \int_V \dot{\psi} dv. \tag{112}$$

Note that, being deviatoric, the second order curvature rate tensor extracts the deviatoric part of the couple-stress tensor. In the present paper, the free energy density ψ has contributions from both the elastic strain and second-order distortion fields. Its simplest possible form is:

$$\psi = \psi(\boldsymbol{\epsilon}_e, \mathbf{G}_e) = \psi(\boldsymbol{\epsilon}_e, \boldsymbol{\kappa}_e, \mathbf{G}_e^{sym}). \tag{113}$$

By differentiating Eq.(113) with respect to time, the rate $\dot{\psi}$ of the free energy density is found as:

$$\dot{\psi} = \frac{\partial \psi}{\partial \boldsymbol{\epsilon}_e} : \dot{\boldsymbol{\epsilon}}_e + \frac{\partial \psi}{\partial \mathbf{G}_e} \vdots \dot{\mathbf{G}}_e = \frac{\partial \psi}{\partial \boldsymbol{\epsilon}_e} : \dot{\boldsymbol{\epsilon}}_e + \frac{\partial \psi}{\partial \boldsymbol{\kappa}_e} : \dot{\boldsymbol{\kappa}}_e + \frac{\partial \psi}{\partial \mathbf{G}_e^{sym}} \vdots \dot{\mathbf{G}}_e^{sym}. \tag{114}$$

Writing the strain and second-order distortion tensors as the sums of their elastic and plastic components, and combining Eqs.(111,114), we then obtain

$$D = \int_V (\dot{\boldsymbol{\epsilon}}_e : (\mathbf{T}^{sym} - \frac{\partial \psi}{\partial \boldsymbol{\epsilon}_e}) + \dot{\boldsymbol{\epsilon}}_p : \mathbf{T}^{sym} + \dot{\mathbf{G}}_e \vdots (\mathbf{M} - \frac{\partial \psi}{\partial \mathbf{G}_e}) + \dot{\mathbf{G}}_p \vdots \mathbf{M}) dv, \tag{115}$$

or alternatively, using Eq.(112):

$$\begin{aligned} D = \int_V (&\dot{\boldsymbol{\epsilon}}_e : (\mathbf{T}^{sym} - \frac{\partial \psi}{\partial \boldsymbol{\epsilon}_e}) + \dot{\boldsymbol{\epsilon}}_p : \mathbf{T}^{sym} + \dot{\boldsymbol{\kappa}}_e : (\tilde{\mathbf{M}}^{dev} - \frac{\partial \psi}{\partial \boldsymbol{\kappa}_e}) + \dot{\boldsymbol{\kappa}}_p : \tilde{\mathbf{M}}^{dev} + ... \\ &... + \dot{\mathbf{G}}_e^{sym} \vdots (\mathbf{M}^{sym} - \frac{\partial \psi}{\partial \mathbf{G}_e^{sym}}) + \dot{\mathbf{G}}_p^{sym} \vdots \mathbf{M}^{sym}) dv. \end{aligned} \tag{116}$$

In reversible elastic processes, the dissipation vanishes. Therefore, we find from Eq.(115)

$$\mathbf{T}^{sym} = \frac{\partial \psi}{\partial \boldsymbol{\epsilon}_e} \tag{117}$$

$$\mathbf{M} = \frac{\partial \psi}{\partial \mathbf{G}_e}, \tag{118}$$

or alternatively from Eq.(116):

$$\tilde{\mathbf{M}}^{dev} = \frac{\partial \psi}{\partial \boldsymbol{\kappa}_e}, \text{ or } \mathbf{M}^{skew} = \frac{\partial \psi}{\partial \mathbf{G}_e^{skew}} \tag{119}$$

$$\mathbf{M}^{sym} = \frac{\partial \psi}{\partial \mathbf{G}_e^{sym}}. \tag{120}$$

Eqs.(117,118) are elastic constitutive relationships for the symmetric part of the Cauchy stress tensor and the hyper-stress tensor, respectively. Alternatively, the latter may be split into the constitutive relationships (119,120) for the deviatoric part of the couple-stress tensor and the symmetric part of the hyper-stress tensor. All these relations are valid for compatible and incompatible anisotropic linear elasticity. Note once again that, although the skew-symmetric part of the Cauchy stress tensor and the hydrostatic part of the couple-stress tensor are needed to maintain the balance of equilibrium of the body, they do not contribute to the free energy, and as such cannot be constitutively specified. As already mentionned, we restrict ourselves to linear constitutive relations. Hence, following Upadhyay et al. [2016], the quadratic form of the free energy is chosen

$$\begin{aligned}\psi = &\frac{1}{2}\boldsymbol{\epsilon}_e : \mathbf{C} : \boldsymbol{\epsilon}_e + \boldsymbol{\epsilon}_e : \mathbf{B} \vdots \tilde{\boldsymbol{\kappa}}_e + \tilde{\boldsymbol{\kappa}}_e \vdots \mathbf{D} : \boldsymbol{\epsilon}_e + \frac{1}{2}\tilde{\boldsymbol{\kappa}}_e \vdots \mathbf{A} \vdots \tilde{\boldsymbol{\kappa}}_e + \boldsymbol{\epsilon}_e : \mathbf{E} \vdots \boldsymbol{\zeta}_e + ... \\ &... + \boldsymbol{\zeta}_e \vdots \mathbf{F} : \boldsymbol{\epsilon}_e + \tilde{\boldsymbol{\kappa}}_e \vdots \mathbf{H} \vdots \boldsymbol{\zeta}_e + \boldsymbol{\zeta}_e \vdots \mathbf{J} \vdots \tilde{\boldsymbol{\kappa}}_e + \frac{1}{2}\boldsymbol{\zeta}_e \vdots \mathbf{K} \vdots \boldsymbol{\zeta}_e,\end{aligned} \tag{121}$$

where the tensors of elastic constants $\mathbf{A}$ through $\mathbf{F}$ and $(\mathbf{H}, \mathbf{J}, \mathbf{K})$ are fourth, fifth or sixth order tensors, as indicated by the total number of dots in the related inner products. The elastic constants are symmetric in indices shared with the strain and symmetric second-order distortion tensors, and skew-symmetric in indices shared with the third-order curvature tensor. The constitutive laws obtained from the derivatives of the free energy in Eqs.(117,119,120) are

$$\mathbf{T}^{sym} = \mathbf{C} : \boldsymbol{\epsilon}_e + \mathbf{B} \vdots \tilde{\boldsymbol{\kappa}}_e + \tilde{\boldsymbol{\kappa}}_e \vdots \mathbf{D} + \mathbf{E} \vdots \boldsymbol{\zeta}_e + \boldsymbol{\zeta}_e \vdots \mathbf{F} \tag{122}$$

$$\mathbf{M}^{skew} = \mathbf{A} \vdots \tilde{\boldsymbol{\kappa}}_e + \boldsymbol{\epsilon}_e : \mathbf{B} + \mathbf{D} : \boldsymbol{\epsilon}_e + \mathbf{H} \vdots \boldsymbol{\zeta}_e + \boldsymbol{\zeta}_e \vdots \mathbf{J} \tag{123}$$

$$\mathbf{M}^{sym} = \mathbf{K} \vdots \boldsymbol{\zeta}_e + \boldsymbol{\epsilon}_e : \mathbf{E} + \mathbf{F} : \boldsymbol{\epsilon}_e + \tilde{\boldsymbol{\kappa}}_e \vdots \mathbf{H} + \mathbf{J} \vdots \tilde{\boldsymbol{\kappa}}_e. \tag{124}$$

Simple arguments on the dimensions of the elastic moduli tensors $(\mathbf{A}, \mathbf{B})$, and $\mathbf{D}$ through $\mathbf{K}$ show that they involve characteristic length scales, and these relations are therefore

non-local in nature. The derivation of the elastic moduli is presented in appendix A for isotropic elasticity, following the procedures detailed in [Upadhyay et al., 2016; Suiker and Chang, 2000]. Positive definiteness of the quadratic form imposes symmetry relations also detailed in the appendix. Additional symmetry relations result from centro-symmetry of the crystalline structure. However, isotropy and centro-symmetry generally do not hold in crystal areas where dislocations and g-disclinations are present. In the latter case, the elastic moduli strongly depend on the presence of defects, as was shown for example for the shear and Young's moduli in the presence of twist boundaries [Wolf and Lutsko, 1989]. The exhaustive determination of the first and second-order elastic moduli in the defected areas is a challenging task, and we indicate in the appendix what could be the main steps.

Using Eqs.(115,117,118), the volumetric dissipation now reads

$$D = \int_V (\dot{\boldsymbol{\epsilon}}_p : \mathbf{T}^{sym} + \dot{\mathbf{G}}_p \vdots \mathbf{M}) dv. \tag{125}$$

Substituting Eqs.(80,85) in Eq.(125), we find:

$$D = \int_V ((\boldsymbol{\alpha} \times \mathbf{V}_\alpha)^{sym} : \mathbf{T}^{sym} + (\boldsymbol{\pi} \times \mathbf{V}_\pi) \vdots \mathbf{M} + \mathbf{grad}\, \dot{\mathbf{U}}_s \vdots \mathbf{M}) dv. \tag{126}$$

Therefore the dissipation can be cast into the form:

$$D = \int_V (\mathbf{F}_\alpha . \mathbf{V}_\alpha + \mathbf{F}_\pi . \mathbf{V}_\pi + \mathbf{grad}\, \dot{\mathbf{U}}_s \vdots \mathbf{M}) dv \tag{127}$$

involving the defect velocities $(\mathbf{V}_\alpha, \mathbf{V}_\pi)$, and where

$$\mathbf{F}_\alpha = \mathbf{T}^{sym} . \boldsymbol{\alpha} : \mathbf{X} \tag{128}$$

$$\mathbf{F}_\pi = \mathbf{M}^t : \boldsymbol{\pi} : \mathbf{X}. \tag{129}$$

$(\mathbf{F}_\alpha, \mathbf{F}_\pi)$ are the driving forces responsible for the motion of the defect densities $(\boldsymbol{\alpha}, \boldsymbol{\pi})$, measured in $N.m^{-3}$ units. Because they do not act on mass elements but on lattice defects in elementary volumes, $(\mathbf{F}_\alpha, \mathbf{F}_\pi)$ are not Newtonian forces. They may be called "configurational forces" [Gurtin, 2008; Maugin, 1995] and have nonlocal character. $\mathbf{F}_\alpha$ is the celebrated Peach-Koehler force, which drives the transport of dislocation densities. Eq.(129) suggests that the motion of g-disclinations is not driven by the stress field but by the second-order hyper-stress field. Positive dissipation is in order for all anelastic processes, which requires that $(\mathbf{F}_\alpha, \mathbf{F}_\pi, \mathbf{M})$ satisfy:

$$\mathbf{F}_\alpha . \mathbf{V}_\alpha \geq 0,\ \mathbf{F}_\pi . \mathbf{V}_\pi \geq 0,\ \mathbf{M} \vdots \mathbf{grad} \dot{\mathbf{U}}_s \geq 0 \tag{130}$$

in Eq.(127), at any time and any point in domain V. The simplest possible constitutive choice for the driving forces allowing to satisfy the inequalities (130) is:

$$\mathbf{F}_\alpha = B_\alpha \mathbf{V}_\alpha; B_\alpha \geq 0,\ \mathbf{F}_\pi = B_\pi \mathbf{V}_\pi; B_\pi \geq 0, \mathbf{M} = B_s\, \mathbf{grad}\, \dot{\mathbf{U}}_s; B_s \geq 0 \tag{131}$$

where (B_α, B_π, B_s) are non-negative coefficients, to which one may assign a constitutive behavior depending on the relevant physics in the operating conditions, such as viscous drag of the moving defects or thermal activation mechanisms related to obstacle overcoming.

7 Solution algorithms

In this Section, we detail algorithms for the solution of the boundary value problem in a body containing a prescribed distribution of dislocations and g-disclinations and submitted to external loading. In a first step, we consider the conservative elasto-static case where the crystal defects are motionless and, in a second step, the dissipative dynamic-anelastic case where the crystal defects are moving with respect to the material.

7.1 Elasto-static incompatible media

We assume that the elastic body V contains a distribution of dislocations/g-disclinations $(\boldsymbol{\alpha}, \boldsymbol{\pi})$. Provisionally, we are not interested in the dynamic anelastic processes that led to this distribution. The body is in equilibrium under loads leading to prescribed displacements $\mathbf{u}$ and distortions $\mathbf{U}$ on a part ∂V_u of its external surface, and traction vectors $\mathbf{t}$ and hyper-traction tensors $\boldsymbol{\Lambda}$ applied on the remaining part ∂V_t of S. From the above, the following equations are therefore satisfied:

$$\begin{aligned}
\mathbf{curl}\,\mathbf{G}_e &= \boldsymbol{\pi} && (132)\\
\mathbf{curl}\,\mathbf{U}_e - \mathbf{G}_e^{\perp} : \mathbf{X} &= \boldsymbol{\alpha} && (133)\\
\mathbf{T}^{sym} &= \frac{\partial \psi}{\partial \boldsymbol{\epsilon}_e} && (134)\\
\mathbf{M} &= \frac{\partial \psi}{\partial \mathbf{G}_e} && (135)\\
\mathbf{div}\,(\mathbf{T}^{sym} - \mathbf{div}\,\mathbf{M}) &= 0 && (136)\\
\mathbf{T}^{skew} + \mathbf{div}\,\mathbf{M}^{skew} &= 0, && (137)
\end{aligned}$$

where Eqs.(134,135) summarize the constitutive relations (122-124). The boundary conditions are

$$\begin{aligned}
\mathbf{t} &= (\mathbf{T} - \mathbf{div}\,\mathbf{M}^{sym}).\mathbf{n} && (138)\\
\boldsymbol{\Lambda} &= \mathbf{M}.\mathbf{n} && (139)
\end{aligned}$$

on ∂V_t and

$$\mathbf{u}_e = \mathbf{u}^d \text{ and } \mathbf{U}_e = \mathbf{U}^d \qquad (140)$$

on ∂V_u. We first solve for the incompatible parts $\mathbf{U}_e^{\perp}$ and $\mathbf{G}_e^{\perp}$ of the elastic distortion and second-order distortion resulting from the presence of the crystal defect fields $(\boldsymbol{\alpha}, \boldsymbol{\pi})$

according to Eqs.(132,133). Invoking the Stokes-Helmholtz orthogonal decomposition of a square-integrable tensor field with square-integrable first order derivatives (see Jiang [1998], theorem 5.8), unique tensor fields $\boldsymbol{\phi}$ and $\mathbf{Z}$ exist (up to a constant for the latter, both fields being square-integrable as well as their derivatives to second order) such that the elastic second-order distortion field $\mathbf{G}_e$ reads as the sum:

$$\mathbf{G}_e = \mathbf{curl}\,\boldsymbol{\phi} + \mathbf{grad}\,\mathbf{Z}, \tag{141}$$

where $(\boldsymbol{\phi}, \mathbf{Z})$ satisfy the orthogonality condition $\int_V \mathbf{curl}\,\boldsymbol{\phi} : \mathbf{grad}\,\mathbf{Z}\, dv = 0$. Taking the curl of $\mathbf{G}_e$ in Eq.(141) extracts $\mathbf{curl}\,\boldsymbol{\phi}$ and leaves out $\mathbf{grad}\,\mathbf{Z}$, whereas taking its divergence extracts $\mathbf{grad}\,\mathbf{Z}$ and discards $\mathbf{curl}\,\boldsymbol{\phi}$. Therefore, Eq.(132) involves only $\mathbf{curl}\,\boldsymbol{\phi}$, which we identify below as the incompatible part $\mathbf{G}_e^{\perp}$ of $\mathbf{G}_e$:

$$\mathbf{curl}\,\mathbf{G}_e^{\perp} = \mathbf{curl}\,\mathbf{curl}\,\boldsymbol{\phi} = \boldsymbol{\pi}. \tag{142}$$

Similarly, $\mathbf{grad}\,\mathbf{Z}$ is the compatible part $\mathbf{G}_e^{\parallel}$ of the elastic second-order distortion $\mathbf{G}_e$, and $\mathbf{Z}$ the elastic distortion $\mathbf{U}_e$, up to a constant. To ensure correctness of this identification, $\mathbf{G}_e^{\perp}$ must vanish identically throughout the body when $\boldsymbol{\pi} = 0$. In this aim, following [Jiang, 1998; Acharya and Roy, 2006], Eq.(142) is augmented with the side conditions:

$$\begin{aligned} \mathbf{div}\,\mathbf{G}_e^{\perp} &= 0 \text{ in } V & (143)\\ \mathbf{G}_e^{\perp}.\mathbf{n} &= 0 \text{ on } \partial V & (144) \end{aligned}$$

with unit normal $\mathbf{n}$ on ∂V. Then taking the curl of Eq.(132) and using the side condition (143), it follows that:

$$\mathbf{curl}\,\mathbf{curl}\,\mathbf{G}_e^{\perp} = \mathbf{grad}\,\mathbf{div}\,\mathbf{G}_e^{\perp} - \mathbf{div}\,\mathbf{grad}\,\mathbf{G}_e^{\perp} = -\mathbf{div}\,\mathbf{grad}\,\mathbf{G}_e^{\perp} = \mathbf{curl}\,\boldsymbol{\pi}. \tag{145}$$

Therefore, $\mathbf{G}_e^{\perp}$ satisfies the Poisson equation

$$\begin{aligned} \mathbf{div}\,\mathbf{grad}\,\mathbf{G}_e^{\perp} &= -\mathbf{curl}\,\boldsymbol{\pi} \text{ in } V & (146)\\ \mathbf{G}_e^{\perp}.\mathbf{n} &= 0 \text{ on } \partial V. & (147) \end{aligned}$$

As a consequence, the field of incompatible elastic second-order distortion $\mathbf{G}_e^{\perp}$ is uniquely determined once the g-disclination density field $\boldsymbol{\pi}$ is prescribed. In particular, it vanishes uniformly when $\boldsymbol{\pi} = 0$. In turn, the Stokes-Helmholtz decomposition of the elastic distortion $\mathbf{U}_e$:

$$\mathbf{U}_e = \mathbf{U}_e^{\perp} + \mathbf{U}_e^{\parallel} = \mathbf{curl}\,\boldsymbol{\psi} + \mathbf{grad}\,\mathbf{w}, \tag{148}$$

can be used to separate its compatible part, $\mathbf{U}_e^{\parallel}$, from its incompatible part, $\mathbf{U}_e^{\perp}$, and to ensure uniqueness of the latter through the solution of a Poisson equation. In the decomposition (148), $\mathbf{U}_e^{\parallel} = \mathbf{grad}\,\mathbf{w}$ belongs again to the null-space of the curl operator since $\mathbf{curl}\,\mathbf{grad}\,\mathbf{w} = 0$, while $\mathbf{U}_e^{\perp} = \mathbf{curl}\,\boldsymbol{\psi}$ must additionally satisfy the side conditions:

$$\begin{aligned} \mathbf{div}\mathbf{U}_e^{\perp} &= 0 \text{ in } V & (149)\\ \mathbf{U}_e^{\perp}.\mathbf{n} &= 0 \text{ on } \partial V. & (150) \end{aligned}$$

Invoking again the identity $\mathbf{curl\ curl}\ \mathbf{U}_e^\perp = \mathbf{grad\ div}\ \mathbf{U}_e^\perp - \mathbf{div\ grad}\ \mathbf{U}_e^\perp$, taking the curl of Eq.(133) and using Eq.(149) then leads to the Poisson equation:

$$\begin{aligned} \mathbf{div\ grad}\ \mathbf{U}_e^\perp &= -\mathbf{curl}\ (\boldsymbol{\alpha} + \mathbf{G}_e^\perp : \mathbf{X}) \text{ in } V & (151)\\ \mathbf{U}_e^\perp.\mathbf{n} &= 0 \text{ on } \partial V. & (152) \end{aligned}$$

Hence, $\mathbf{U}_e^\perp$ is uniquely determined once the dislocation and g-disclination density fields $(\boldsymbol{\alpha}, \boldsymbol{\pi})$ are prescribed. In particular, it vanishes uniformly in V when $\boldsymbol{\alpha} = 0$ and $\boldsymbol{\pi} = 0$.

The solutions $(\mathbf{U}_e^\perp, \mathbf{G}_e^\perp)$ generally do not allow satisfying mechanical equilibrium. Therefore, we now proceed with the solution for the compatible part $\mathbf{u}_e^\parallel$ of the elastic displacement, which has to be tailored to fulfill the equilibrium equations (136,137) and boundary conditions (138,139,140). Separating the compatible and incompatible parts, we can rewrite the elasto-static field equations (134,135,136) in the form of a partial differential equation of Navier type in V:

$$\mathbf{div}\ (\mathbf{T}^{\parallel,sym} - \mathbf{div}\,\mathbf{M}^\parallel) + \mathbf{f}^\perp = 0, \tag{153}$$

where $\mathbf{T}^\parallel$ and $\mathbf{M}^\parallel$ denote the stress and hyper-stress tensors resulting from the compatible parts $(\boldsymbol{\epsilon}_e^\parallel, \mathbf{G}_e^\parallel)$ of the elastic strain and second-order distortion tensors, and the volumetric force density $\mathbf{f}^\perp$ is:

$$\mathbf{f}^\perp = \mathbf{div}\ (\mathbf{T}^{\perp,sym} - \mathbf{div}\,\mathbf{M}^\perp). \tag{154}$$

In the latter, $\mathbf{T}^{\perp,sym}$ and $\mathbf{M}^\perp$ denote the symmetric stress and hyper-stress tensors resulting from the incompatible elastic strain and second-order distortion tensors $(\boldsymbol{\epsilon}_e^\perp, \mathbf{G}_e^\perp)$ determined above from the solution of the Poisson equations (146,151). Hence, $\mathbf{f}^\perp$ reflects the incompatibility arising from the presence of defects. The boundary conditions following from Eqs.(138,139,140) are

$$\begin{aligned} \mathbf{u}_e^\parallel &= \mathbf{u}^d \text{ on } \partial V_u & (155)\\ \mathbf{U}_e^\parallel &= \mathbf{U}^d - \mathbf{U}_e^\perp \text{ on } \partial V_u & (156)\\ (\mathbf{T}^\parallel - \mathbf{div}\,\mathbf{M}^{sym,\parallel}).\mathbf{n} &= \mathbf{t} - (\mathbf{T}^\perp - \mathbf{div}\,\mathbf{M}^{sym,\perp}).\mathbf{n} \text{ on } \partial V_t & (157)\\ \mathbf{M}^\parallel.\mathbf{n} &= \boldsymbol{\Lambda} - \mathbf{M}^\perp.\mathbf{n} \text{ on } \partial V_t. & (158) \end{aligned}$$

Taken together, Eqs.(153,154) and the boundary conditions (155-158) set a fourth-order Navier-type elasticity problem for the unknown field $\mathbf{u}_e^\parallel$. The skew-symmetric part $\mathbf{M}^{skew}$ of the hyper-stress tensor follows from constitutive specifications, while the still-undetermined skew-symmetric part of the stress tensor $\mathbf{T}^{skew}$ derives only from the balance equation (137). Such solutions were obtained in [Berbenni et al., 2014] for twin tips by using Fast Fourier Transforms techniques, in a framework restricted to first-order with a symmetric Cauchy stress tensor given by the standard Hooke's law for isotropic elasticity.

7.2 Anelastic incompatible media

Gathering the above analyzes, the equations of the boundary value problem for anelasticity in incompatible media can be summarized as follows:

$$\begin{aligned}
\mathbf{curl}\,\mathbf{G}_e^{\perp} &= \boldsymbol{\pi} && (159)\\
\mathbf{curl}\,\mathbf{U}_e^{\perp} - \mathbf{G}_e^{\perp} : \mathbf{X} &= \boldsymbol{\alpha} && (160)\\
\mathbf{T}^{sym} &= \frac{\partial \psi}{\partial \boldsymbol{\epsilon}_e} && (161)\\
\mathbf{M} &= \frac{\partial \psi}{\partial \mathbf{G}_e} && (162)\\
\mathbf{div}\,(\mathbf{T}^{sym} - \mathbf{div}\,\mathbf{M}) &= 0 && (163)\\
\mathbf{T}^{skew} + \mathbf{div}\,\mathbf{M}^{skew} &= 0, && (164)\\
\dot{\mathbf{U}}_p &= \boldsymbol{\alpha} \times \mathbf{V}_\alpha && (165)\\
\dot{\mathbf{G}}_p &= \boldsymbol{\pi} \times \mathbf{V}_\pi + \mathbf{grad}\,\dot{\mathbf{U}}_s && (166)\\
\dot{\boldsymbol{\alpha}} &= -\mathbf{curl}\,\dot{\mathbf{U}}_p + \dot{\mathbf{G}}_p^{\perp} : \mathbf{X} && (167)\\
\dot{\boldsymbol{\pi}} &= -\mathbf{curl}\,\dot{\mathbf{G}}_p && (168)\\
\mathbf{V}_\alpha &= \frac{1}{B_\alpha}\,\mathbf{T}^{sym}.\boldsymbol{\alpha} : \mathbf{X} && (169)\\
\mathbf{V}_\pi &= \frac{1}{B_\pi}\,\mathbf{M}^t : \boldsymbol{\pi} : \mathbf{X}, && (170)\\
\mathbf{grad}\,\dot{\mathbf{U}}_s &= \frac{1}{B_s}\mathbf{M} && (171)
\end{aligned}$$

where Eqs.(161,162) summarize the constitutive relations (122-124), and Eqs.(169,170) generically govern the velocity of dislocations and g-disclinations. As in Section 7.1, the boundary conditions are prescribed on the compatible displacement/distortion fields and the traction vector and hyper-traction tensor at the external surfaces of the body:

$$\begin{aligned}
\mathbf{u}^{\parallel} &= \mathbf{u}^d \quad \text{on}\,\partial V_u && (172)\\
\mathbf{U}^{\parallel} &= \mathbf{U}^d - \mathbf{U}_e^{\perp} \quad \text{on}\,\partial V_u && (173)\\
(\mathbf{T}^{\parallel} - \mathbf{div}\,\mathbf{M}^{sym,\parallel}).\mathbf{n} &= \mathbf{t} - (\mathbf{T}^{\perp} - \mathbf{div}\,\mathbf{M}^{sym,\perp}).\mathbf{n}\,\text{on}\,\partial V_t && (174)\\
\mathbf{M}^{\parallel}.\mathbf{n} &= \boldsymbol{\Lambda} - \mathbf{M}^{\perp}.\mathbf{n}\,\text{on}\,\partial V_t. && (175)
\end{aligned}$$

However, Eqs.(172-175) differ substantially from the corresponding boundary conditions (155-158) in the elasto-static problem, because $\mathbf{u}^{\parallel}$ and $\mathbf{U}^{\parallel}$ now include an evolving anelastic part. Boundary conditions on the dislocation/g-disclination density tensors may additionally be prescribed.

The unknown fields of the problem are the compatible displacement field $\mathbf{u}^{\parallel}$ and the crystal defect fields $(\boldsymbol{\alpha}, \boldsymbol{\pi})$. Suppose an arbitrary distribution of crystal defects is known at the

initial time, and let the compatible parts of the anelastic strain and second-order distortion tensors arbitrarily set to zero at this time, without loss of generality. Then, following the methods in Section 7.1, the incompatible components $(\boldsymbol{\epsilon}_e^{\perp}, \mathbf{G}_e^{\perp})$ can be obtained from the solution of Eqs.(159,160). Substituting the latter in Eqs.(161,162) to compute $\mathbf{T}^{\perp,sym}$ and $\mathbf{M}^{\perp}$, and in turn substituting $\mathbf{T}^{\perp,sym}$ and $\mathbf{M}^{\perp}$ in the balance equation (163) sets out a fourth-order Navier-type equation for the compatible part of the elastic displacement $\mathbf{u}_e^{\parallel}$ with Eqs.(172-175) as boundary conditions. Note once again that $\mathbf{T}^{skew}$ is determined only from the moment of momentum balance equation (164). In parallel, the compatible parts of Eqs.(165,166) provide the updated values $(\boldsymbol{\epsilon}_p^{\parallel}, \mathbf{G}_p^{\parallel})$ of the anelastic strain and second-order distortion from the fluxes of dislocations and g-disclinations. Adding to the latter their elastic counterparts allows finding the (compatible) distortion $\mathbf{U}^{\parallel}$ and displacement $\mathbf{u}^{\parallel}$ from Eqs.(27,33), up to a constant chosen from the boundary condition (172). Finally, the updated values of the crystal defect densities are generated from the incompatible parts of the anelastic strain and second-order distortion rate tensors, through the transport equations (167,168) and the constitutive relationships (169,170) for defect mobility. From this point onward, the procedure is iterated at the next time step. The numerical implementation may couple a conventional Galerkin Finite Element scheme for the solution of the equilibrium problem with a mixed Galerkin-Least Squares Finite Element algorithm for the solution of the crystal defects transport problem (see the references [Roy and Acharya, 2005; Varadhan et al., 2006]), or by combining spectral approaches for the solution of the equilibrium and transport problems [Berbenni et al., 2014; Djaka et al., 2015; Upadhyay et al., 2016; Djaka et al., 2017].

8 Case study of symmetrical tilt boundaries

With the aim of discussing below the distribution of dislocations and generalized disclinations in symmetrical tilt boundaries, either straight or presenting ledges, we now present a restriction of the above equations to a plane model with all defect lines normal to the plane.

8.1 A plane dislocation/g-disclination model

In the orthonormal frame $(\mathbf{e}_1, \mathbf{e}_2, \mathbf{e}_3)$, we consider a distribution of g-disclinations with lines parallel to $\mathbf{e}_3$: $\boldsymbol{\pi} = \pi_{ij3}\mathbf{e}_i \otimes \mathbf{e}_j \otimes \mathbf{e}_3, (i,j) \in (1,2)$, all other components being zero. Such a distribution reflects a situation where only in-plane distortion jumps $[\![U_{ij}]\!], (i,j) \in (1,2)$ are allowed, namely shear strain jumps $[\![\epsilon^e_{12}]\!]$, stretch jumps $([\![\epsilon^e_{11}]\!], [\![\epsilon^e_{22}]\!])$ and $[\![\omega^e_3]\!]$ rotation jumps. In this setting, the continuity condition (68) implies that $\pi_{ij3,3} = 0$. Thus the g-disclination density fields only depend on the coordinates (x_1, x_2): $\pi_{ij3} = \pi_{ij3}(x_1, x_2)$, $(i,j) \in (1,2)$, and are therefore in a plane state. In component form, the incompatibility equation (64) reads: $\pi_{ijk} = e_{klm}G^e_{ijm,l} = -e_{klm}G^p_{ijm,l}$, which reduces here

to

$$\pi_{ij3} = G^e_{ij2,1} - G^e_{ij1,2} = G^p_{ij1,2} - G^p_{ij2,1}. \tag{176}$$

Hence, the only relevant elastic and plastic second-order distortion components are: $(G^e_{ijk}, (i,j,k) \in (1,2))$ and $(G^p_{ijk}, (i,j,k) \in (1,2))$. The relevant plastic second order distortion rates (80) are therefore

$$\dot{G}^p_{ij1} = -\pi_{ij3} V^\pi_2 + \dot{U}^s_{ij,1}, \tag{177}$$

$$\dot{G}^p_{ij2} = +\pi_{ij3} V^\pi_1 + \dot{U}^s_{ij,2}, (i,j) \in (1,2), \tag{178}$$

where (V^π_1, V^π_2) are the in-plane g-disclination velocity components and $(\dot{U}^s_{ij,k}, (i,j,k) \in (1,2))$ the complementary compatible second-order distortion rate components. The transport equations for g-disclination densities (80) read, in component form

$$\dot{\pi}_{ij3} = \dot{G}^p_{ij1,2} - \dot{G}^p_{ij2,1} = -(\pi_{ij3} V^\pi_2)_{,2} - (\pi_{ij3} V^\pi_1)_{,1} \tag{179}$$

Using the expressions (129) of the Peach-Koehler-type forces and the constitutive equations (131) for the g-disclination velocities provides their relations with the hyper-stresses:

$$V^\pi_1 = +\frac{1}{B_\pi} \pi_{rs3} M_{rs2} \tag{180}$$

$$V^\pi_2 = -\frac{1}{B_\pi} \pi_{rs3} M_{rs1}, \ (r,s) \in (1,2). \tag{181}$$

Similarly, the complementary gradient components $\dot{U}^s_{ij,k}$ are related with the hyper-stresses through:

$$\dot{U}^s_{ij,1} = \frac{1}{B_s} M_{ij1} \tag{182}$$

$$\dot{U}^s_{ij,2} = \frac{1}{B_s} M_{ij2}, \ (i,j) \in (1,2). \tag{183}$$

Using Eqs.(180,181), the transport equations (179) now read

$$\dot{\pi}_{ij3} = \frac{1}{B_\pi} [(\pi_{ij3} \pi_{rs3} M_{rs1})_{,2} - (\pi_{ij3} \pi_{rs3} M_{rs2})_{,1}], \ (i,j,r,s) \in (1,2). \tag{184}$$

Similarly, the dislocation transport equation (86) is, in component form

$$\dot{\alpha}_{ij} = -e_{jkl} \dot{U}^p_{il,k} + \dot{G}^{p,\perp}_{ikl} = -e_{jkl} \dot{U}^p_{il,k} + s^\alpha_{ij}. \tag{185}$$

The source terms s^α_{ij} are limited to

$$s^\alpha_{i3} = \dot{G}^p_{i12} - \dot{G}^p_{i21} = \pi_{i13} V^\pi_1 + \pi_{i23} V^\pi_2, \ i \in (1,2). \tag{186}$$

Therefore, only edge dislocations (α_{i3}, $i \in (1,2)$) are generated by the motion of the ($\pi_{i13}, \pi_{i23}, i \in (1,2)$) g-disclinations. The only non-zero plastic distortion rate components are:

$$\dot{U}^p_{i2} = +\alpha_{i3} V^\alpha_1 \tag{187}$$
$$\dot{U}^p_{i1} = -\alpha_{i3} V^\alpha_2, \tag{188}$$

and the relevant dislocation transport equations read

$$\dot{\alpha}_{i3} = -(\alpha_{i3} V^\alpha_1)_{,1} - (\alpha_{i3} V^\alpha_2)_{,2} + \pi_{i13} V^\pi_1 + \pi_{i23} V^\pi_2,\ i \in (1,2). \tag{189}$$

Thus, if all other dislocation densities are initially absent, the dislocation distribution only involve the edge components (α_{13}, α_{23}). Then, the continuity equation (70) implies

$$\alpha_{i3,3} = \pi_{ikk} = 0,\ i \in (1,2), \tag{190}$$

meaning that the dislocation distribution is also in a plane state: $\alpha_{i3} = \alpha_{i3}(x_1, x_2)$, $i \in (1,2)$. Using the expressions (129) of the Peach-Koehler-type forces on dislocation densities, the constitutive equations (131) for the dislocation velocities and the relations (180,181), we find for the dislocation transport equations (189):

$$\begin{aligned} \dot{\alpha}_{13} &= -\frac{1}{B_\alpha}(T^{sym}_{12}\alpha^2_{13} + T^{sym}_{22}\alpha_{13}\alpha_{23})_{,1} + \frac{1}{B_\alpha}(T^{sym}_{12}\alpha_{13}\alpha_{23} - T^{sym}_{11}\alpha^2_{13})_{,2} ... \\ &... + \frac{1}{B_\pi}(\pi_{113}\pi_{ij3}M_{ij2} - \pi_{123}\pi_{ij3}M_{ij1}) \end{aligned} \tag{191}$$

$$\begin{aligned} \dot{\alpha}_{23} &= -\frac{1}{B_\alpha}(T^{sym}_{12}\alpha_{13}\alpha_{23} + T^{sym}_{22}\alpha^2_{23})_{,1} + \frac{1}{B_\alpha}(T^{sym}_{12}\alpha^2_{23} + T^{sym}_{11}\alpha_{13}\alpha_{23})_{,2} ... \\ &... + \frac{1}{B_\pi}(\pi_{213}\pi_{ij3}M_{ij2} - \pi_{223}\pi_{ij3}M_{ij1}),\ (i,j) \in (1,2). \end{aligned} \tag{192}$$

Eqs.(184,191,192) suggest that the relevant stress and hyper-stress components are (T_{ij}, M_{ij1}, M_{ij2}), $(i,j) \in (1,2)$. The Mindlin-Eshel balance equations (100,101) therefore reduce to

$$T^{sym}_{11,1} + T^{sym}_{12,2} = (M_{111,1} + M_{112,2})_{,1} + (M_{121,1} + M_{122,2})_{,2} \tag{193}$$
$$T^{sym}_{21,1} + T^{sym}_{22,2} = (M_{211,1} + M_{212,2})_{,1} + (M_{221,1} + M_{222,2})_{,2} \tag{194}$$
$$2T^{skew}_{21} = (M_{121} - M_{211})_{,1} + (M_{122} - M_{212})_{,2}. \tag{195}$$

The only non-vanishing couple-stress components are: $\tilde{M}_{31} = (M_{211} - M_{121})/2$ and $\tilde{M}_{32} = (M_{212} - M_{122})/2$. Hence, Eqs.(195) also reads:

$$2T^{skew}_{21} = -(\tilde{M}_{31,1} + \tilde{M}_{32,2}) \tag{196}$$

in terms of couple-stresses, and reducing Eqs.(193,194) to their Mindlin-Tiersten counterparts:

$$T^{sym}_{11,1} + T^{sym}_{12,2} = -\frac{1}{2}(\tilde{M}_{31,1} + \tilde{M}_{32,2})_{,2} \quad (197)$$

$$T^{sym}_{21,1} + T^{sym}_{22,2} = +\frac{1}{2}(\tilde{M}_{31,1} + \tilde{M}_{32,2})_{,1} \quad (198)$$

is legitimate when the relations (109):

$$M_{111,1} + M_{112,2} = 0 \quad (199)$$

$$(M_{121,1} + M_{122,2}) + (M_{211,1} + M_{212,2}) = 0 \quad (200)$$

$$M_{221,1} + M_{222,2} = 0 \quad (201)$$

are satisfied. Indeed, the hyper-stress components ($M^{sym}_{ijk}\,(i,j,k) \in (1,2)$) are determined from these equations and boundary conditions on the hyper-tractions $\mathbf{\Lambda}^{sym}$, while the stress and hyper-stress components (T_{ij}, M^{skew}_{ijk}, $(i,j,k) \in (1,2)$) are obtained independently from Eqs.(196,197,198). Clearly, the M^{sym}_{ijk} cannot be determined from the Mindlin-Tiersten equations (196,197,198) when the constraints (199,200,201) are not satisfied.

Finally, the imposed boundary conditions may include plane traction vectors and hyper-traction tensors $\mathbf{\Lambda}^{sym}$ involving plane stretch and shear, with components independent of x_3. Gathering all the above results on the relevant stresses, hyper-stresses, elastic distortions and second-order distortions, it is seen that the linear elastic constitutive laws have the general form

$$T^{sym}_{ij} = c_{(ij)(kl)}\epsilon^e_{kl} + d_{(ij)klm}G^e_{klm} \quad (202)$$

$$M_{ijk} = a_{ijklmn}G^e_{lmn} + b_{ijk(lm)}\epsilon^e_{lm},\ (i,j,k,l,m,n) \in (1,2), \quad (203)$$

where ϵ^e_{kl} denotes the $kl-th$ component of the elastic strain tensor and parentheses in the index rows indicate symmetry of the elastic constants with respect to the involved indexes. Hence, a plane state of stress, elastic strain and second-order distortion is shown to take place.

8.2 Symmetrical tilt boundaries

As an example of the plane state of incompatibility detailed above in Section 8.1, we now analyze the straight $\Sigma5(310)[001]$ symmetrical tilt boundary in a Cu bicrystal. This boundary was already investigated by Cahn et al. [2006] using atomistic calculations and Fressengeas et al. [2014] from the point of view of standard disclinations, but new features are revealed by the present work. To generate this boundary, two adjacent perfect

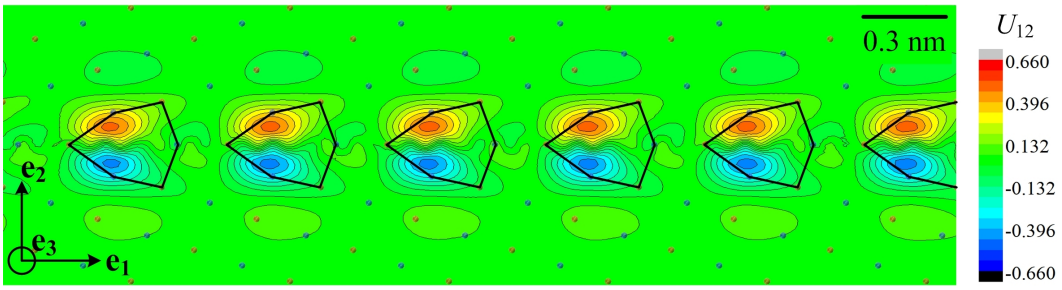

Figure 1: U^e_{12} elastic distortion field along a straight $\Sigma 5(310)$ symmetrical tilt boundary in a Cu bicrystal misoriented by a 36.87° angle about the [001] direction, superimposed on the atomic lattice. Sharp variations interpreted as discontinuities $[\![U^e_{12}]\!]$ can be noticed along the boundary. Black lines highlight atomic structural units.

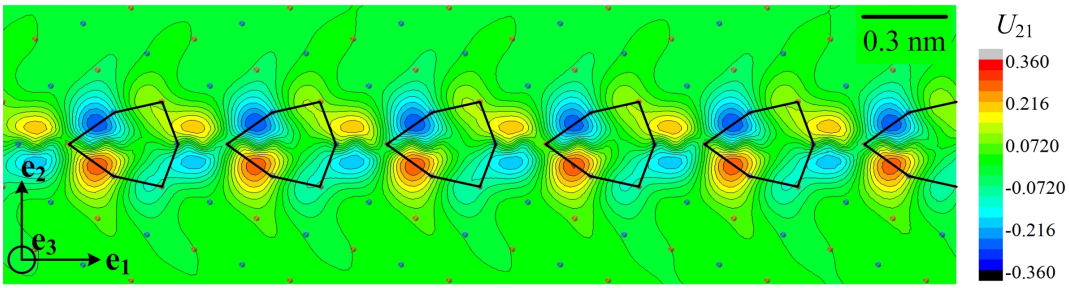

Figure 2: U^e_{21} elastic distortion field along a straight $\Sigma 5(310)$ symmetrical tilt boundary in a Cu bicrystal misoriented by a 36.87° angle about the [001] direction, superimposed on the atomic lattice. Sharp variations interpreted as discontinuities $[\![U^e_{21}]\!]$ can be noticed along the boundary. Black lines highlight atomic structural units.

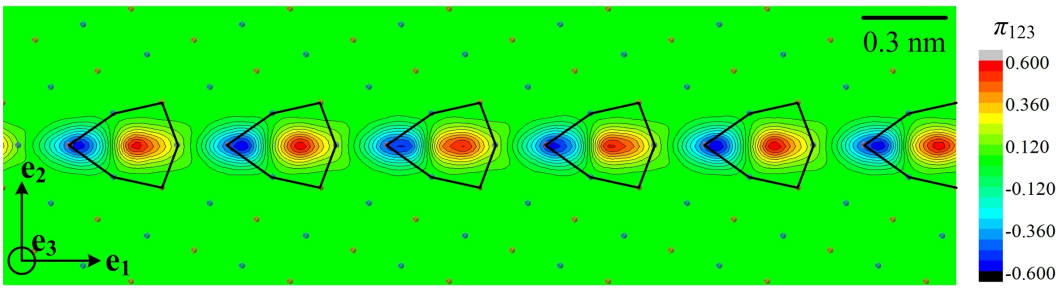

Figure 3: π_{123} g-disclination field along a straight $\Sigma 5(310)$ symmetrical tilt boundary in a Cu bicrystal misoriented by a 36.87° angle about the [001] direction, superimposed on the atomic lattice. Note the continuity of the g-disclination field along the boundary. Black lines highlight atomic structural units.

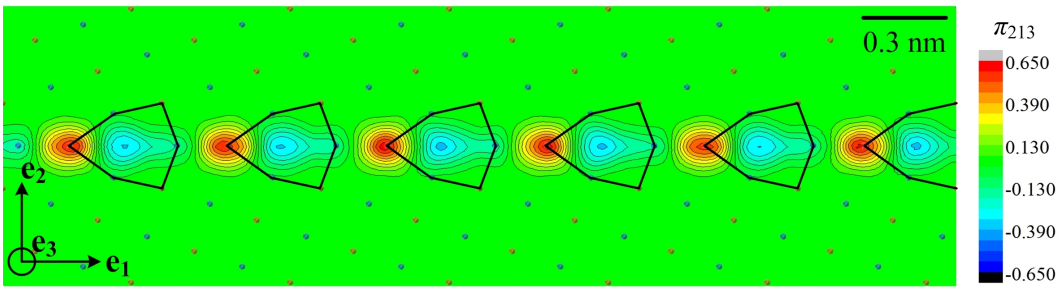

Figure 4: π_{213} g-disclination field along a straight $\Sigma 5(310)$ symmetrical tilt boundary in a Cu bicrystal misoriented by a 36.87° angle about the [001] direction, superimposed on the atomic lattice. Note the continuity of the g-disclination field along the boundary. Black lines highlight atomic structural units.

copper crystals were first separately rotated symmetrically about the [001] axis, the bottom one by an angle $-\theta/2$ and the top one by $+\theta/2$. The extremities of both crystals were then cut and joined together with respect to coincidence site lattice points to create the initial configuration of the bicrystal. As it is arbitrarily set up, this configuration needs relaxation to a lesser energy configuration by rearrangement of the atomic positions. The molecular dynamics LAMMPS simulation code [Plimpton, 1995] and the empirical embedded-atoms method (EAM) interatomic potential developed by Mishin et al. [2001] were used in this aim. The sample contains 1624 atoms and has dimensions $7.8nm, 6.5nm$ and $0.72nm$ along the orthonormal basis $(\mathbf{e}_1, \mathbf{e}_2, \mathbf{e}_3)$, respectively. Periodic boundary conditions were applied in all three directions. The relaxation process used the conjugate gradient method, and the final configuration was thermally balanced for $60ps$ by using a Nosé-Hoover thermostat [Martyna et al., 1994] at $1K$ to avoid thermal noise. Several trials were made from different initial configurations and the final configuration with the lowest energy was retained. Then, following the discrete-to-continuum method detailed in Sun et al. [2016, 2018], elastic displacement, distortion and second-order distortion fields were built, on the basis of the atomic displacements between the initial and final configurations, in a continuum superimposed to the atomic configuration at the same scale. The analysis reveals a plane state of distortion and second-order distortion along the $(\mathbf{e}_1, \mathbf{e}_2)$ symmetry plane of the boundary, and localized areas where the elastic displacement and distortion fields encounter sharp jumps interpreted as discontinuities across the boundary[1]. For example, the distortion fields (U^e_{12}, U^e_{21}) and the discontinuities $([\![U^e_{12}]\!], [\![U^e_{21}]\!])$

[1]The issue of whether a discrete distortion data set should be regarded as reflecting a continuously differentiable field or if surfaces of discontinuity exist along grain boundaries, and how are the second-order distortion and g-disclination density tensors fields built in the latter case, was treated in [Fressengeas and Beausir, 2019] in the context of the experimental determination of standard disclinations at mesoscale. The issue ultimately boils down to how numerical differentiation of the first and second-order distortion data sets should be carried out at grain boundaries, and the analysis and methods presented in this paper

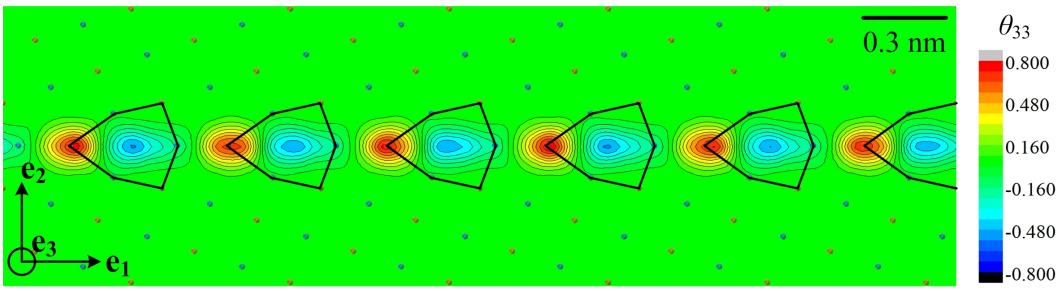

Figure 5: $\theta_{33} = (\pi_{213} - \pi_{123})/2$ wedge disclination density field along a straight $\Sigma 5(310)$ symmetrical tilt boundary in a Cu bicrystal misoriented by a 36.87° angle about the [001] direction, superimposed on the atomic lattice. Black lines highlight atomic structural units.

are shown in Figs.(1,2). Through the incompatibility of the second-order distortion and using Eq.(176), these discontinuities can be converted into the periodic arrays of smooth g-disclination dipoles (π_{123}, π_{213}) shown in Figs.(3,4) in an intermediate layer less than $1nm$ thick.

As a consequence of the rotation discontinuity $[\![\omega^e_{12}]\!] = ([\![U^e_{12} - U^e_{21}]\!])/2$ deduced from the above, periodic standard wedge disclination $\theta_{33} = (\pi_{213} - \pi_{123})/2$ dipole arrays shown here in Fig.5 can be evidenced in this layer. They are similar those proposed in Fressengeas et al. [2014] to model symmetrical tilt boundaries in the framework of the mechanics of dislocation and standard disclination fields [Fressengeas et al., 2011]. The disclination density field θ_{33} reflects the rotational incompatibility along the boundary, but the g-disclination fields (π_{123}, π_{213}) also reflect the incompatibility of the symmetric part of the second-order distortion arising from the discontinuities $[\![\epsilon^e_{12}]\!] = ([\![U^e_{12} + U^e_{21}]\!])/2$ of the elastic shear strain field shown in Fig.6. The periodic patterns seen in this figure are in qualitative agreement with the shear strain discontinuities observed in a $\Sigma 9(122)$ tilt boundary in a silicon bicrystal by applying geometric phase analysis to atomic resolution images obtained from scanning transmission electron microscopy [Couillard et al., 2013]. Both the experimental and simulated shear discontinuity patterns bear witness to the presence of periodic g-disclination dipole arrays complementing the description of straight symmetrical tilt boundaries with standard disclination dipoles. Note finally that no significant elastic stretch discontinuity $[\![U^e_{11}]\!]$ or $[\![U^e_{22}]\!]$ has been observed along such boundaries.

consequently apply to the present case.

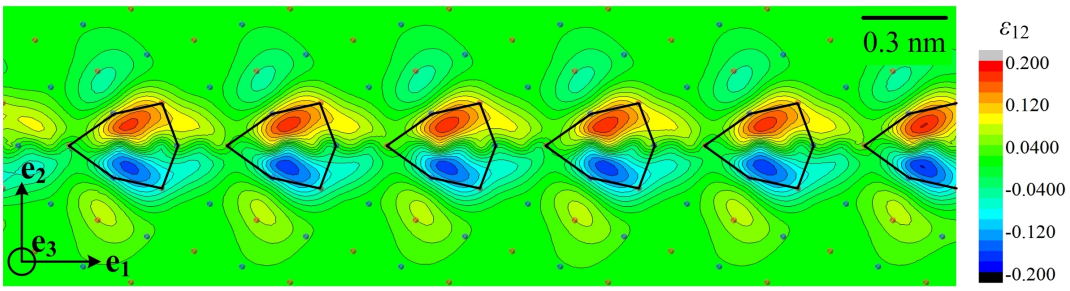

Figure 6: ϵ^e_{12} elastic strain field along a straight $\Sigma5(310)$ symmetrical tilt boundary in a Cu bicrystal misoriented by a 36.87° angle about the [001] direction, superimposed on the atomic lattice. Black lines highlight atomic structural units.

8.3 Ledges in symmetrical tilt boundaries

Observations suggest that grain boundaries involve various defects affecting their microstructure and dynamics, such as atomic inclusions, kinks and ledges [McDowell, 2010]. In the presence of ledges, the migration of a grain boundary under stress is unlikely to happen normally to itself over large planar areas. Rather, small patches bounded by ledge loops are expected to spread side-ward through tangential motion of the loops. Such a mechanism was recently observed in grain boundary migration under shear stress in ultra-fine-grained materials [Rajabzadeh et al., 2013, 2014]. Ledges have been modeled as "disconnections", and characterized by a combined dislocation and step character [Hirth, 1994; Hirth and Pond, 1996]. A crystallographic analysis allows identifying the Burgers vector of the dislocation and the height of the step from the displacement shift complete (DSC) lattice of the bicrystal. However, being of purely geometric nature, such an analysis does not allow capturing the dynamic properties of ledges [Cahn et al., 2006]. As indicators of displacement and strain discontinuities across bounded surfaces, dislocation and generalized disclination fields offer an alternative to disconnections for a correct elastostatic description of ledges but, similar to dislocations and in contrast to disconnection steps, the generalized discinations are additionally endowed with a dissipative dynamics through the transport laws (80), the driving forces (129) and mobility laws (131). These properties allow for a complete dynamic description of ledges within the framework of the present theory.

In this Section, we describe the salient aspects of the elastic structure of a $\Sigma5(310)[001]$ symmetrical tilt boundary containing a ledge loop by using the mechanical framework of the dislocation and generalized disclination density fields detailed above. The boundary was obtained as follows from the straight boundary shown above in Section 8.2. At first, half of the $\Sigma5(310)[001]$ straight boundary was moved downward, which yielded an unrelaxed configuration. Then, a relaxation process similar to that presented above was used

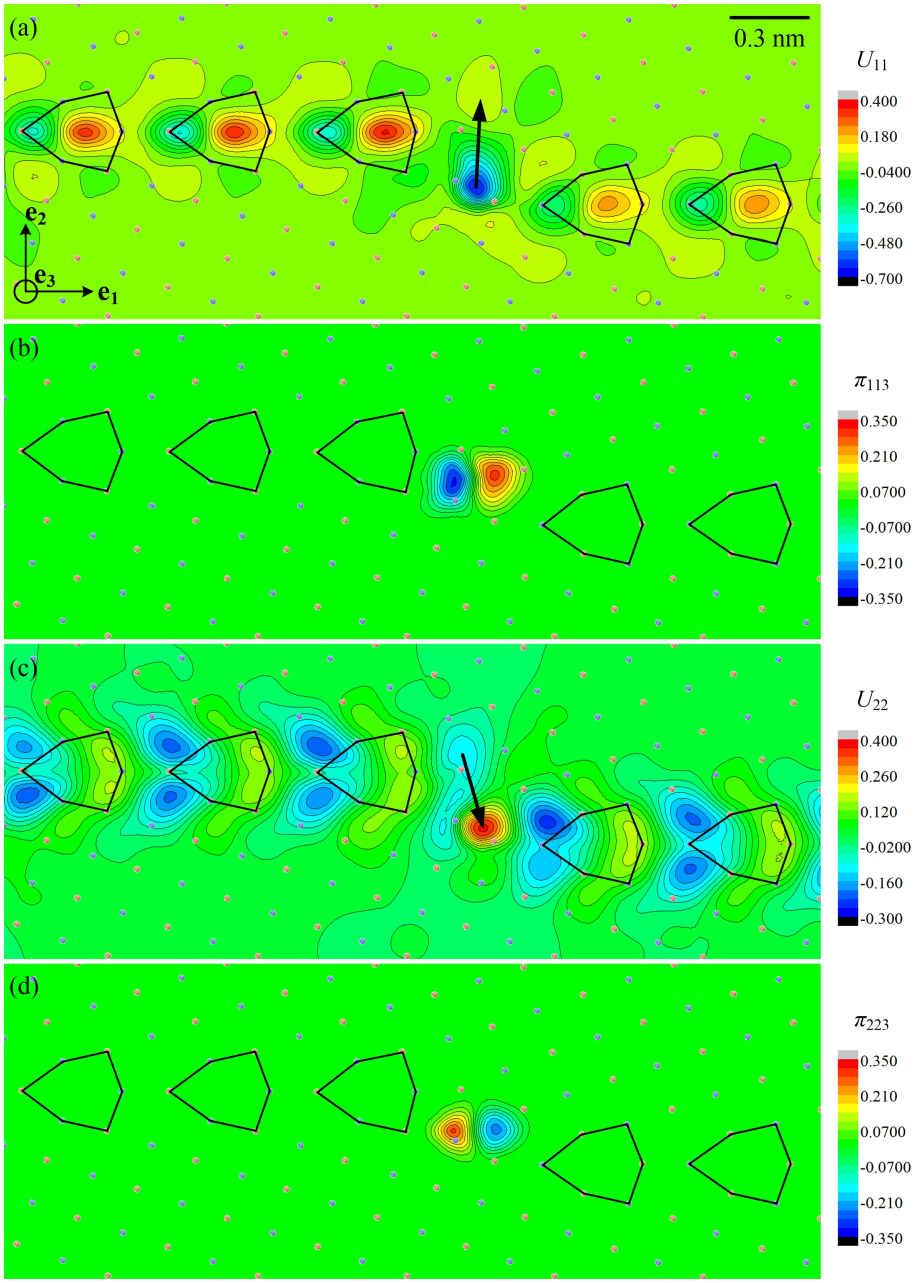

Figure 7: Elastic distortion and g-disclination density fields superimposed on the atomic lattice along a stepped $\Sigma5(310)$ symmetrical tilt boundary in a *Cu* bicrystal misoriented by a 36.87° angle about the [001] direction, superimposed on the atomic lattice: (a) U^e_{11} field; (b) π_{113} g-disclination field; (c) U^e_{22} field; (d) π_{223} g-disclination field. Black lines highlight atomic structural units and black arrows the localized spots of (U^e_{11},U^e_{22}) in the ledge.

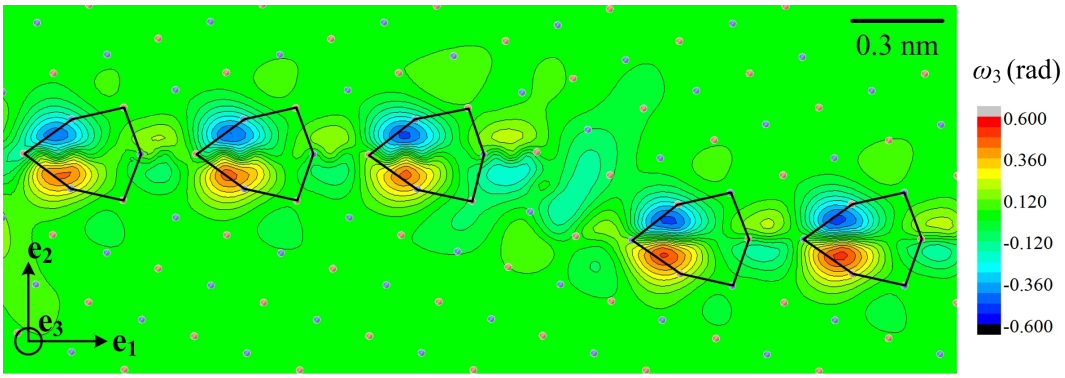

Figure 8: ω_3^e rotation field superimposed on the atomic lattice along a stepped $\Sigma5(310)$ symmetrical tilt boundary in a Cu bicrystal misoriented by a 36.87° angle about the [001] direction, superimposed on the atomic lattice. Black lines highlight atomic structural units.

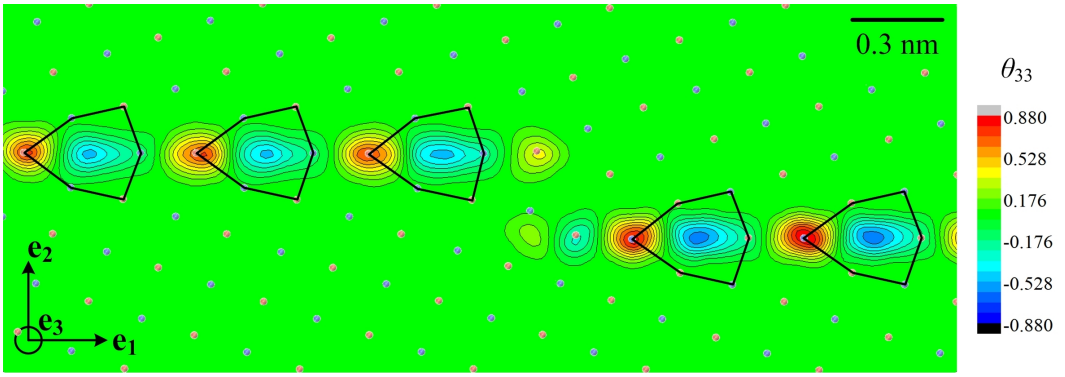

Figure 9: θ_{33} disclination density field superimposed on the atomic lattice along a stepped $\Sigma5(310)$ symmetrical tilt boundary in a Cu bicrystal misoriented by a 36.87° angle about the [001] direction, superimposed on the atomic lattice. Black lines highlight atomic structural units.

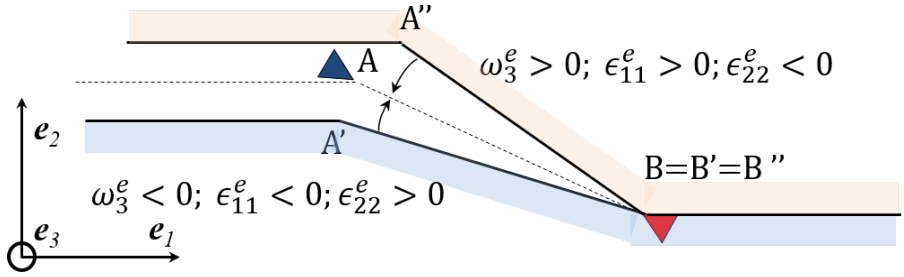

Figure 10: Sketch of a ledge. The blue and red triangles represent negative and positive wedge disclinations at points A and B respectively. The boundary was cut from the left of the figure to point B. As a result, the positive wedge disclination in B opens a rotational gap in the material. The negative disclination in A fills the gap from the left of the figure to point A. Since $A'B' \neq A''B''$, strain discontinuities $([\![\epsilon_{11}^e]\!], [\![\epsilon_{22}^e]\!])$ appear when welding back $A'B'$ and $A''B''$ along AB.

to acquire the lowest energy configuration. As Fig.7 shows, the atomic structural units exhibit symmetry with respect to the interface and are only slightly distorted as passed by the ledge, whose height is of the order of 2 Å. The most striking features are shown in Fig.7.a.c by the stretch fields $U_{11}^e = \epsilon_{11}^e$ and $U_{22}^e = \epsilon_{22}^e$. Both are continuous across the interface, except in the ledge areas where fast variations highlighted by black arrows and interpreted as discontinuities $([\![U_{11}^e]\!], [\![U_{22}^e]\!])$ can be noticed. As mentioned above, stretch discontinuities are not seen with such intensity along straight tilt boundaries, and they appear to be localized in ledges. In terms of g-disclination densities, they are reflected by the strong π_{113} and π_{223} dipoles present in the ledge area in Fig.7.b.d. In contrast, the ω_3^e rotation field and the corresponding θ_{33} standard wedge disclination field shown respectively in Fig.8 and Fig.9 are only slightly affected by the presence of the ledge. Fig.9 noticeably shows however that the ledge area contains a wedge dipole at angle with the normal to the interface. The sketch drawn in Fig.10 provides an interpretation of the ledge in terms of generalized disclination dipoles. In the figure, the grain boundary has been cut from the left of the figure to point B. As a result, the positive wedge disclination θ_{33} in B (red triangle) has been opening a rotational gap in the material. The figure shows the configuration obtained when the negative wedge disclination in A (blue triangle) has been filling this gap from the left of the figure to point A. The grain boundary will be completely welded back when the ledge segments $A'B'$ and $A''B''$ of the lower and upper grains are merged again along AB. In this rotation and stretch process, $(\omega_3^e > 0, \epsilon_{11}^e > 0, \epsilon_{22}^e < 0)$ in the upper grain, whereas $(\omega_3^e < 0, \epsilon_{11}^e < 0, \epsilon_{22}^e > 0)$ in the lower grain, as Fig.(7.a.c) and Fig.8 also show, so that discontinuities $[\![\omega_3^e]\!]$ and $([\![\epsilon_{11}^e]\!], [\![\epsilon_{22}^e]\!])$ appear along AB and translate into θ_{33} disclination and (π_{113}, π_{223}) g-disclination dipoles. Note that in the mesoscale approach of Fressengeas [2019] where the dislocation fields

are taken into consideration but not the g-disclinations, Burgers vector conservation requires that the stretch jumps $([\![\epsilon^e_{11}]\!], [\![\epsilon^e_{22}]\!])$ be offset by some curvature of the interface. Ledges are manifestations at nanoscale of interface curvature at mesoscale. Similarly, their representation using g-disclination dipoles may be seen as a counterpart at nanoscale of interface curvature modeling at mesoscale.

9 Conclusion

The paper presented a second-order linearized field theory of crystal defects: dislocations and generalized disclinations, able to accommodate arbitrary discontinuities of the elastic displacement vector and distortion (strain and rotation) tensor fields, and to describe continuously the anelasticity (plasticity and phase transformation) of crystalline solids. It is a "linearized" theory because it uses the additive decomposition of the distortion into strain and rotation, and a "second-order" theory because it accounts for the incompatibility of the second-order elastic distortion field, by taking advantage of the duality existing between this incompatibility and the discontinuity of the elastic distortion field. The generalized disclination densities are defined as the continuous variables carrying this second-order incompatibility. The field theory of dislocations and standard disclinations of Fressengeas et al. [2011], to which the present theory reduces when the symmetric part of the second-order elastic distortion (*i.e.* the elastic strain-gradient) retains compatibility, is also a second-order theory in this sense, but it can only account for the incompatibility of the elastic curvature field reflected in the standard disclination density field. By dealing with discontinuities of the elastic strain field, the present theory naturally finds applications in modeling incoherent boundaries and interfaces between materials of dissimilar lattice structures and symmetries.

Most of the above features are common with the earlier papers presenting g-disclinations [Acharya and Fressengeas, 2012, 2015]. Here however, in contrast with these references, the account for the materials dynamics in the presence of dislocation and g-disclination fields uses the full second-order distortion rate $\dot{\mathbf{G}}$ tensor fields, which appears as a kinematic variable in the power of internal forces. The work-conjugate fields $(\mathbf{T}^{sym}, \mathbf{M})$ to the strain rate tensor $\dot{\boldsymbol{\epsilon}}$ and second-order distortion rate tensor $\dot{\mathbf{G}}$, respectively the symmetric stress tensor and hyper-stress tensor fields, are consequently involved in the mechanical balance equations. Accordingly, the boundary conditions involve arbitrary traction vector and second order hyper-traction tensor fields applied to the external surface of the body. The present approach may therefore be seen as an extension of the gradient theory of Mindlin and Eshel [1968] to incompatible media. Because it deals with compatible elastic strain and second-order distortion tensor fields, the latter appears as a limit of the present theory in the absence of dislocations and g-disclinations. Following further this path, the

elastic strain and second-order elastic distortion (strain-"gradient" and curvature) tensors are chosen as the kinematic objects rendering the state of deformation of the lattice in the presence of dislocations and g-disclinations. As a result of these choices, the elastic constitutive laws relate the symmetric part of the stress tensor and the hyper-stress tensor to the elastic strain and second-order distortion tensors. These laws are provided in the appendix for isotropic materials.

Involving second-order distortion incompatibility vastly increases the interest of a "strain-gradient" theory. In particular, the present theory allows coping with the core properties of crystal defects such as grain boundaries when the latter are viewed at a sufficiently small scale. This was shown above from the examples of straight and stepped $\Sigma5(310)[001]$ symmetrical tilt boundaries in Cu. The description of the grain boundaries used the distortion and second-order distortion fields, as obtained from atomic displacements by the discrete-to-continuum method of Sun et al. [2016, 2018]. Discontinuities in the displacement, rotation and strain fields were found across the boundaries, pointing at the presence of dislocation and g-disclination fields in these areas. Features unexpected in straight symmetrical tilt boundaries were discussed, such as the presence of localized shear discontinuities and the induced g-disclination dipoles. Along stepped tilt boundaries, significant rotation and stretch discontinuities were observed in the ledge areas, leading in particular to characteristic g-disclination dipole patterns. As a result, ledges have an elastic energy not only from the incompatible strain field associated with dislocations, but also from the incompatible second-order distortion field associated with the g-disclination dipoles. Their elastic properties and interactions with other crystal defects may therefore be described by using the elastostatic equations of the present mechanical theory of dislocation and g-disclination fields.

Further interest in considering continuous dislocation and g-disclination density fields for plasticity and phase transformation modeling arises from the dynamic framework that derives from the conservation of the Burgers vector and elastic distortion tensor discontinuity during their motion across arbitrary patches, and from the associated transport laws. Being unquestionable from a kinematic point of view, the transport equations for dislocation and g-disclination densities provide a natural basis for the description of plasticity and phase transformation through dislocation glide and interface/interphase motion. They allow introducing a well-posed set of partial differential equations for the dynamics of the compatible displacement and crystal defect density fields, whose hyperbolic character confers propagative properties to both plasticity and phase transformation. Examples of solutions for the evolution of dislocation and disclination density fields in straight tilt boundaries were provided in [Taupin et al., 2013, 2014; Cordier et al., 2014] with applications to shear-coupled boundary migration in various materials. Such a framework also allows scaling up the dynamics of defect ensembles from individual defects to polycrystalline scale, through seamless coarse-graining procedures [Acharya and Roy, 2006;

Taupin et al., 2015]. Hence, concrete physical situations where the above constructs could be useful are commonplace in polycrystalline ice, rocks and metals.

A
Appendix: Elasticity in isotropic media

In this appendix, we provide the elasticity tensors $(\mathbf{A}, \mathbf{B}, \mathbf{C}, \mathbf{D}, \mathbf{E}, \mathbf{F}, \mathbf{H}, \mathbf{J}, \mathbf{K})$ defined in Eqs.(121-124) in isotropic media. Clearly, these tensors cannot account for the elasticity of crystals at small scale, due to local lattice anisotropy. The presence of crystal defects further limits their applicability at this scale due to centro-symmetry breaking. However, they may be used as a simple benchmark for the comparison of different solutions. In [Upadhyay et al., 2016], the tensors $(\mathbf{A}, \mathbf{B}, \mathbf{C}, \mathbf{D})$ were derived in the special case where the body is subjected to surface tractions and moments, but not to symmetric hyper-tractions, so that the symmetric part of the elastic second-order distortion vanishes. The results are recalled below in terms of the second-order elastic curvature tensor $\boldsymbol{\kappa}_e$ and couple-stress tensor $\tilde{\mathbf{M}}$:

$$\mathbf{T}^{sym} = \lambda tr(\boldsymbol{\epsilon}_e) + 2\mu\boldsymbol{\epsilon}_e + B_1(\boldsymbol{\kappa}_e^{dev})^{sym} \tag{A-1}$$

$$\tilde{\mathbf{M}}^{dev} = B_1\boldsymbol{\epsilon}_e^{dev} + A_1\boldsymbol{\kappa}_e^{dev} - A_2(\boldsymbol{\kappa}_e^{t})^{dev}. \tag{A-2}$$

Here, (λ, μ) are the usual Lamé constants and (A_1, A_2, B_1) are three elastic coefficients leading to independent contributions to the free energy density ψ. The cross-contributions of curvature to the symmetric stress, and of strain to the deviatoric couple-stress vanish in the case of centro-symmetry ($B_1 = 0$), in particular in the absence of lattice defects. The remaining tensors $(\mathbf{E}, \mathbf{F}, \mathbf{H}, \mathbf{J}, \mathbf{K})$ involve contributions of the symmetric second-order distortion to the free energy density. We obtained their expressions by applying the methodology of Suiker and Chang [2000] to build n^{th}-order isotropic tensors. They turn out to be:

$$E_{(ij)(kl)m} = E_1(e_{ikm}\delta_{jl} + e_{jkm}\delta_{il} + e_{ilm}\delta_{jk} + e_{jlm}\delta_{ik}) \tag{A-3}$$

$$F_{(ij)k(lm)} = F_1(e_{ikl}\delta_{jm} + e_{jkl}\delta_{im} + e_{ikm}\delta_{jl} + e_{jkm}\delta_{il}) \tag{A-4}$$

$$\begin{aligned} H_{[ij]k(lm]n} &= H_1\delta_{lm}(\delta_{ik}\delta_{jn} - \delta_{in}\delta_{jk}) + H_2(\delta_{mn}(\delta_{ik}\delta_{jl} - \delta_{il}\delta_{jk}) - \delta_{ln}(\delta_{ik}\delta_{jm}... \\ ... &- \delta_{im}\delta_{jk})) + H_3(\delta_{kl}(\delta_{im}\delta_{jn} - \delta_{in}\delta_{jm}) + \delta_{km}(\delta_{il}\delta_{jn} - \delta_{in}\delta_{jl})) \end{aligned} \tag{A-5}$$

$$\begin{aligned} J_{(ij)k[lm]n} &= J_1\delta_{ij}(\delta_{kl}\delta_{mn} - \delta_{km}\delta_{ln}) + J_2(\delta_{mn}(\delta_{ik}\delta_{jl} + \delta_{il}\delta_{jk}) - \delta_{ln}(\delta_{ik}\delta_{jm}... \\ ... &+ \delta_{im}\delta_{jk})) + J_3(\delta_{kl}(\delta_{im}\delta_{jn} + \delta_{in}\delta_{jm}) - \delta_{km}(\delta_{il}\delta_{jn} + \delta_{in}\delta_{jl})) \end{aligned} \tag{A-6}$$

$$\begin{aligned} K_{(ij)k(lm)n} &= K_1(\delta_{ij}(\delta_{kl}\delta_{mn} + \delta_{km}\delta_{ln}) + \delta_{lm}(\delta_{in}\delta_{jk} + \delta_{ik}\delta_{jn})) + K_2\delta_{ij}\delta_{kn}\delta_{lm} + ... \\ ... &+ K_3(\delta_{ik}(\delta_{jl}\delta_{mn} + \delta_{jm}\delta_{ln}) + \delta_{jk}(\delta_{im}\delta_{ln} + \delta_{il}\delta_{mn})) + ... \\ ... &+ K_4(2\delta_{ik}\delta_{jm}\delta_{ln} + \delta_{ij}(\delta_{km}\delta_{ln} + 2\delta_{kl}\delta_{mn}) + \delta_{lm}(\delta_{ik}\delta_{jn} + 2\delta_{in}\delta_{jk})) + ... \\ ... &+ K_5\delta_{kn}(\delta_{il}\delta_{jm} + \delta_{im}\delta_{jl}) + ... \\ ... &+ K_6(\delta_{in}(\delta_{jl}\delta_{km} + \delta_{jm}\delta_{kl}) + \delta_{jn}(\delta_{il}\delta_{km} + \delta_{im}\delta_{kl})). \end{aligned} \tag{A-7}$$

Parentheses in the groups of subscripts indicate symmetry relative to these subscripts, brackets indicate skew-symmetry. The conditions ($E_1 = F_1, J_1 = -H_1, H_2 = J_2 = 0, J_3 =$

$-H_3$) are necessary and sufficient for the symmetry of the quadratic form ψ, because they guarantee $E_{ijklm} = F_{klmij}$ and $H_{ijklmn} = J_{lmnijk}$. Hence, nine additional independent elastic constants arise: (E_1, H_1, H_3) and $(K_i, i = 1, 6)$. Requiring that the energy density ψ be positive definite, we find them to be positive. Like B_1, E_1 has dimension of a stress times a length, whereas (H_1, H_3) and $(K_i, i = 1, 6)$ have dimension of a stress times a squared length, like (A_1, A_2). The involved length necessarily scales with the characteristic length l of the crystal defect areas where the curvatures and strain-gradients are significant, here of the order of 1 Å. Thus, the two groups of constants are of the order of μl and μl^2 respectively.

As indicated in the main text, the exhaustive determination of the first and second-order elastic moduli is a challenging task at small scale in the presence of defects, and we indicate here the main steps to be followed in this endeavor. The task first requires building the small-scale displacement field in the defected areas, for example in the manner of Sun et al. [2016], by using either discrete displacements from atomistic simulations or images obtained through high resolution microscopy and geometric phase analysis [Couillard et al., 2013; Hÿtch et al., 2003]. The derivation of the corresponding elastic distortion and second-order distortion fields follows, as shown in Sun et al. [2016] and exemplified above in Sections (8.2,8.3). The additional input of adequate elastic potentials allows computing the rate of free energy $\dot{\psi}$ from atomistic simulations, for any loading increment. Then Eqs.(114,117,118) give access to the relevant stress and hyper-stress components, and to the first and second order elastic moduli through identification procedures yet to be implemented, but akin to methods developed in Maranganti and Sharma [2007].

References

Acharya, A. (2001). A model of crystal plasticity based on the theory of continuously distributed dislocations. *J. Mech. Phys. Solids*, 49:761–784.

Acharya, A. (2011). Microcanonical entropy and mesoscale dislocation mechanics and plasticity. *J. Elast.*, 104:23–44.

Acharya, A. and Fressengeas, C. (2012). Coupled phase transformations and plasticity as a field theory of deformation incompatibility. *Int. J. Fract.*, 174:87–94.

Acharya, A. and Fressengeas, C. (2015). Continuum mechanics of the interactions between phase boundaries and dislocations in solids. In Chen, G. Q., Grinfeld, M., and Knops, R. J., editors, *Differential Geometry and Continuum Mechanics*, volume 137, pages 125–168. Springer Proceedings in Mathematics and Statistics.

Acharya, A. and Roy, A. (2006). Size effects and idealized dislocation microstructure at small scales: predictions of a phenomenological model of mesoscopic field dislocation mechanics: Part I. *J. Mech. Phys. Solids*, 54:1687–1710.

Berbenni, S., Paliwal, B., and Cherkaoui, M. (2013). A micromechanics-based model for shear-coupled grain boundary migration in bicrystals. *Int. J. Plast.*, 44:68–94.

Berbenni, S., Taupin, V., Djaka, K. S., and Fressengeas, C. (2014). A numerical spectral approach for solving elasto-static field dislocation and g-disclination mechanics. *Int. J. Solids Struct.*, 51:4157–4175.

Bilby, B., Bullough, R., and Smith, E. (1955). Continuous distributions of dislocations: a new application of the methods of non-Riemannian geometry. *Proc. Roy. Soc. London A*, 231:263–273.

Cahn, J. W., Mishin, Y., and Suzuki, A. (2006). Coupling grain boundary motion to shear deformation. *Acta Mater.*, 54:4953–4975.

Cleja-Tigoiu, S., Pascan, R., and Tigoiu, V. (2019). Disclination based model of grain boundary in crystalline materials with microstructural defects. *Int. J. Plast.*, 114:227–251.

Coleman, B. D. and Gurtin, M. E. (1967). Thermodynamics with internal state variables. *J. Chem. Phys.*, 47:597–613.

Cordier, P., Demouchy, S., Beausir, B., Taupin, V., Barou, F., and Fressengeas, C. (2014). Disclinations provide the missing mechanism for deforming olivine-rich rocks in the mantle. *Nature*, 507:51–56.

Couillard, M., Radke, G., and Botton, G. A. (2013). Strain fields around dislocation arrays in a $\Sigma 9$ silicon bicrystal measured by scanning transmission electron microscopy. *Philos. Mag.*, 93:1250–1267.

deWit, R. (1970). Linear theory of static disclinations. In Simmons, J. A., deWit, R., and Bullough, R., editors, *Fundamental aspects of dislocation theory*, volume I, pages 651–673. Nat. Bur. Stand. (US), Spec. Publ. 317.

Djaka, K. S., Taupin, V., Berbenni, S., and Fressengeas, C. (2015). A numerical spectral approach to solve the dislocation density transport equation. *Modell. Simul. Mater. Sci.Eng.*, 23:065008.

Djaka, K. S., Villani, A., Taupin, V., Capolungo, L., and Berbenni, S. (2017). Field dislocation mechanics for heterogeneous elastic materials: a numerical spectral approach. *Comput. Meth. Appl. Mech. Eng.*, 315:921–942.

Fressengeas, C. (2019). Curvature effects on boundary migration. *J. Mech. Phys. Solids*, 124:814–826.

Fressengeas, C. and Beausir, B. (2019). Tangential continuity of the curvature tensor at grain boundaries underpins disclination density determination from spatially mapped orientation data. *Int. J. Solids Struct.*, 156-157:210–215.

Fressengeas, C., Taupin, V., and Capolungo, L. (2011). An elasto-plastic theory of dislocation and disclination fields. *Int. J. Solids Structures*, 48:3499–3509.

Fressengeas, C., Taupin, V., and Capolungo, L. (2014). Continuous modeling of the structure of symmetric tilt boundaries. *Int. J. Solids Structures*, 51:1434–1441.

Fressengeas, C., Taupin, V., Upadhyay, M., and Capolungo, L. (2012). Tangential continuity of elastic/plastic curvature and strain at interfaces. *Int. J. Solids Struct.*, 49:2660–2667.

Fressengeas, C. and Upadhyay, M. V. (2020). A continuum model for slip transfer at grain boundaries. *Adv. Model. and Simul. in Eng. Sci.*, 7:12.

Gurtin, M. E. (2008). A theory of grain boundaries that accounts automatically for grain misorientation and grain-boundary orientation. *J. Mech. Phys. Solids*, 56:640–662.

Hirth, J. P. (1994). Dislocations, steps and disconnections at interfaces. *J. Phys. Chem. Solid.*, 55:985–989.

Hirth, J. P. and Pond, R. C. (1996). Steps, dislocations and disconnections as interface defects relating to structure and phase transformations. *Acta Mater.*, 44:4749–4763.

Hÿtch, M. J., Putaux, J. L., and Pénisson, J. M. (2003). Measurement of the displacement field of dislocations to 0.03 $\mathring{A}$ by electron microscopy. *Nature*, 423:270–273.

Jiang, B. (1998). The least-squares finite element method. In *Theory and Computation in Fluid Dynamics and Electromagnetics, Springer Series in Scientific Computation.* Springer Verlag, Berlin, Heidelberg, New York.

Kondo, K. (1953). On the geometrical and physical foundations of the theory of yielding. In for Theoretical, J. N. C. and Mechanics, A., editors, *Second Japan Nat. Cong. Appl. Mech.*, pages 41–47. Science Council of Japan, Tokyo.

Kröner, E. (1981). Continuum theory of defects. In Balian, R., editor, *Les Houches, Session XXXV, Physics of Defects*, pages 217–314. North-Holland, Amsterdam.

Maranganti, R. and Sharma, P. (2007). A novel atomistic approach to determine strain-gradient elasticity constants: tabulation and comparison for various metals, semiconductors, silica, polymers, and (Ir) relevance for nanotechnologies. *J. Mech. Phys. Solids*, 55:1823–1852.

Martyna, G. J., Tobias, D. J., and Klein, M. L. (1994). Constant pressure molecular dynamics algorithms. *J. Chem. Phys.*, 101:4177–4189.

Maugin, G. A. (1995). Material forces: concepts and applications. *ASME J. Appl. Mech. Rev.*, 48:213–245.

McDowell, D. L. (2010). A perspective on trends in multiscale plasticity. *Int. J. Plast.*, 26:1280–1309.

Mindlin, R. D. (1965). Second gradient of strain and surface-tension in linear elasticity. *Int. J. Solids Structures*, 1:417–438.

Mindlin, R. D. and Eshel, N. N. (1968). On first strain-gradient theories in linear elasticity. *Int. J. Solids Structures*, 4:109–124.

Mindlin, R. D. and Tiersten, H. F. (1962). Effects of couple-stresses in linear elasticity. *Arch. Rat. Mech. Anal.*, 11:415–448.

Mishin, Y., Mehl, M. J. D. A., Papaconstantopoulos, A. F. V., and Kress, J. (2001). Structural stability and lattice defects in copper: ab initio, tight-binding, and embedded-atom calculations. *Phys. Rev. B*, 63:224106.

Nye, J. (1953). Some geometrical relations in dislocated crystals. *Acta Metall.*, 1:153–162.

Plimpton, S. (1995). Fast parallel algorithms for short-range molecular dynamics. *J. Comput. Phys.*, 117:1–19.

Rajabzadeh, A., Legros, M., Combe, N., Mompiou, F., and Molodov, D. A. (2013). Evidence of grain boundary dislocation step motion associated to shear-coupled grain boundary migration. *Philos. Mag.*, A93:1299–1316.

Rajabzadeh, A., Mompiou, F., Legros, M., and Combe, N. (2014). Elementary mechanisms of shear-coupled grain boundary migration. *Phys. Rev. Lett.*, 110:265507.

Roy, A. and Acharya, A. (2005). Finite element approximation of field dislocation mechanics. *J. Mech. Phys. Solids*, 53:143–170.

Simon, T., Kröger, A., Somsen, C., Dlouhy, A., and Eggeler, G. (2010). On the multiplication of dislocations during martensitic transformation in NiTi shape memory alloys. *Acta Mater.*, 58:1850–1860.

Suiker, A. S. J. and Chang, C. S. (2000). Application of higher-order tensor theory for formulating enhanced continuum models. *Acta Mech.*, 142:223–234.

Sun, X. Y., Fressengeas, C., Taupin, V., Cordier, P., and Combe, N. (2018). Disconnections, dislocations and generalized disclinations in grain boundary ledges. *Int. J. Plast.*, 104:134–146.

Sun, X. Y., Taupin, V., Fressengeas, C., and Cordier, P. (2016). Continuous description of the atomic structure of grain boundaries using dislocation and generalized disclination density fields. *Int. J. Plast.*, 77:75–89.

Taupin, V., Capolungo, L., and Fressengeas, C. (2014). Disclination mediated plasticity in shear-coupled boundary migration. *Int. J. Plast.*, 53:179–192.

Taupin, V., Capolungo, L., Fressengeas, C., Das, A., and Upadhyay, M. (2013). Grain boundary modeling using an elasto-plastic theory of dislocation and disclination fields. *J. Mech. Phys. Solids*, 61:370–384.

Taupin, V., Capolungo, L., Fressengeas, C., Upadhyay, M., and Beausir, B. (2015). A mesoscopic theory of dislocation and disclination fields for grain boundary-mediated crystal plasticity. *Int. J. Solids Struct.*, 71:277–290.

Taupin, V., Gbemou, K., Fressengeas, C., and Capolungo, L. (2017). Nonlocal elasticity tensors in dislocation and disclination cores. *J. Mech. Phys. Solids*, 100:62–84.

Upadhyay, M. V., Capolungo, L., Taupin, V., Fressengeas, C., and Lebensohn, R. A. (2016). A higher order elasto-viscoplastic model using Fast Fourier Transforms: effects of lattice curvatures on mechanical response of nanocrystalline metals. *Int. J. Plast.*, 83:126–152.

Varadhan, S., Beaudoin, A. J., Acharya, A., and Fressengeas, C. (2006). Dislocation transport using an explicit Galerkin/least-squares formulation. *Modelling Simul. Mater. Sci. Eng.*, 14:1245–1270.

Vattré, A. (2017a). Elastic strain relaxation in interfacial dislocation patterns: I. A parametric energy-based framework. *J. Mech. Phys. Solids*, 105:254–282.

Vattré, A. (2017b). Elastic strain relaxation in interfacial dislocation patterns: II. From long- and short-range interactions to local reactions. *J. Mech. Phys. Solids*, 105:283–305.

Volterra, V. (1907). Sur l'équilibre des corps élastiques multiplement connexes. *Ann. Sci. Ecol. Norm. Sup.*, III:405–517.

Warner, D. H., Sansoz, F., and Molinari, J. F. (2006). Atomistic based continuum investigation of plastic deformation in nanocrystalline copper. *Int. J. Plast.*, 22:754–774.

Weingarten, J. (1901). Sulle superfici di discontinuita nella teoria dell'elasticita dei corpi solidi. *Atti. Accad. Naz. Lincei, Cl. Sci. Fis. Mat. Natur. Rend. V*, 10:1–57.

Wolf, D. and Lutsko, J. F. (1989). Structurally-induced elastic anomalies in a superlattice of (001) twist grain boundaries. *J. Mater. Res.*, 4:1427–1443.

Zbib, H. M., Overman, C. T., Akasheh, F., and Bahr, D. (2011). Analysis of plastic deformation in nanoscale metallic multilayers with coherent and incoherent interfaces. *Int. J. Plast.*, 27:1618–1639.